FINAL TECHNICAL REPORT

DETAILED MAPPING OF THE NORTHERN SAN ANDREAS FAULT USING LIDAR IMAGERY

Collaborative Research with Judith Zachariasen
and USGS Western Region Earthquake Hazards Team

Principal Investigator:

Judith Zachariasen

488 Kenilworth Ave
San Leandro, CA 94577
Tel: 510-633-9744; Fax: 510-633-9744;
judyzach@comcast.net

now at: URS Corporation
1333 Broadway, Ste 800
Oakland, CA 94612
510-874-1749
judy_zachariasen@urscorp.com

Contributor:

Carol S. Prentice
U.S. Geological Survey
Western Earthquake Hazards
345 Middlefield Road MS/977
Menlo Park, CA 94025;
(650) 329-5690;
cprentice@usgs.gov

Program Element I

Keywords:

Geologic Mapping; Tectonic Geomorphology; Quaternary Fault Behavior; LiDAR

U.S. Geological Survey
National Earthquake Hazards Reduction Program
Award Number 05HQGR0069

June 2008

Research supported by U.S. Geological Survey (USGS), Department of Interior, under USGS award number 03HQGR0069. The views and conclusions contained in this document are those of the authors and should not be interpreted as necessarily representing the official policies, either expressed or implied, of the U.S. Government.

Abstract

We have used airborne LiDAR imagery to compile an updated map of active traces along about 38 km of the northern San Andreas fault in Mendocino and Sonoma Counties. LiDAR is a robust tool for fault mapping in densely vegetated regions because it allows the vegetative cover to be virtually stripped away, yielding high-resolution topographic information about the ground surface beneath the forest canopy. We have used the "bare earth" data to generate digital elevation models (DEMs) of the ground surface on which we have compiled a detailed map of the fault traces and fault-realted geomorphic features. The LiDAR-based DEMs are much higher resolution than existing topographic maps and aerial photographs, allowing us to map the locations of fault traces more accurately than was previously possible. The new maps should aid future site-specific fault studies that can yield information about the characteristics of paleoearthquakes necessary to developing robust seismic hazard models.

The northern San Andreas fault zone in this region is generally narrow and typically comprises multiple, parallel or en echelon strands. Numerous linear valleys, elongate depressions, uphill-facing scarps, and ponds delineate the fault zone. Many of the ponds contain large, dead redwood trees, with deeply submerged roots. We speculate that the trees drowned subsequent to fault rupture and sudden deepening of the ponds. Although there is not a plethora of promising paleoseismic sites, we have identified a few where detailed study could shed light on the size and timing of prehistoric ruptures of this heretofore largely unstudied section of the San Andreas fault.

Introduction

The San Andreas Fault, the dominant plate boundary fault in California, poses a significant hazard to the state. The northern section of the fault, which extends 470 km from San Juan Bautista to the Mendocino triple junction, last ruptured in the 1906, generating a **M** 7.9 earthquake and producing surface rupture with several meters of displacement (Figure 1). The earthquake caused significant damage in San Francisco; damage elsewhere was mitigated by the minimal population and development along the fault. Given the current dense population in San Francisco proper and the growing population in regions that were sparsely developed in 1906, this portion of the fault continues to pose a hazard to San Francisco, and, as development and population has expanded, the level of risk has increased in areas previously little affected. Understanding the nature of rupture on this portion of the fault is thus crucial to quantifying and consequently mitigating the future risk to people and infrastructure.

The earthquake characteristics and history of the northern portion of the San Andreas fault are not well understood and have received little attention compared to the southern portion. Consequently the contribution to seismic hazard from this section is less well constrained. Current statewide hazard models favor 1906-style rupture scenarios in which the entire fault ruptures; other models include repetitive rupture of smaller but defined, discrete segments of the fault (WGCEP, 2003; 2008). However, there are, in fact, few data to support either model, or indeed different models entirely, such as models that do not require the existence of persistent rupture segments. The problem remains relatively unconstrained and current hazard models are largely model- rather than data-driven.

Developing a better-supported model requires information about fault characteristics, including location, complexity and zone width, which can be obtained from detailed fault mapping, and also rupture characteristics, including extent and magnitude, of prehistoric earthquakes, which can be obtained from paleoseismic investigations. Both types of data are lacking for much of the northern San Andreas fault. This is in part due to its relative inaccessibility and the difficulty of mapping in its densely forested terrain. Even aerial photographs, often excellent vehicles for identifying faults from afar, have failed to reveal the details of the fault because they only image the top of the forest canopy. Thus maps of the fault in the northern section have been less detailed and accurate than those of other, less vegetated sections. The consequences of this are that the fault has been less well characterized, the identification of paleoseismic sites that can yield detailed information about the timing and size of prehistoric earthquakes is more difficult, and understanding of the fault is less complete than along other sections of the fault. Better characterization of the fault requires improved fault mapping as well as further paleoseismic studies.

LiDAR (Light Distance and Ranging) technology offers the means by which to overcome some of these obstacles and provide new detail about the location and characteristics of the northern San Andreas fault. The technology permits a laser signal to penetrate the forest canopy and ultimately yield an image of the ground surface as if the forest were stripped away. The level of detail available from LiDAR data is therefore much superior to that of air photos in densely forested regions. In September 2003, NASA provided LiDAR surveys to the USGS of a 70-km long swath of the northern San Andreas fault (Figure 2), allowing unprecedented remote visual access to the geomorphology beneath the forest canopy. These data can help us now overcome some of the obstacles that inaccessibility and limited exposure posed to earlier mappers.

The aim of this research has been to use the 2003 northern San Andreas LiDAR dataset to create a new and refined map of the northern San Andreas fault, precisely locating fault strands and fault-related geomorphic features, as well as identifying promising locations for future paleoseismic investigations that may ultimately yield the kind of data necessary to constrain the timing and recurrence of prehistoric earthquake events on the San Andreas fault.

Seismotectonic Setting and Seismic Hazard

The plate boundary in western California includes numerous dextral and dextral-oblique faults of the San Andreas fault system that accommodate about 75% of the relative plate motion (Argus and Gordon, 2001). The dominant fault within that system is the San Andreas fault, which is broadly divided into northern and southern sections that are characterized by stick-slip behavior with interseismic locking and strain accumulation punctuated by episodic fault rupture and consequent earthquakes; the two portions are separated by a section of fault between Parkfield and San Juan Bautista that is characterized by fault creep. Large coseismic ruptures of the San Andreas fault are considered incapable of extending through the creeping section to link the southern and northern faults in a single event; consequently, the northern and southern San Andreas faults are treated as independent sources in seismic hazard assessments (WGCEP, 2008; WGNCEP, 1996). The northern San Andreas fault extends from the north end of the creeping section near San Juan Bautista to the Mendocino triple junction near Shelter Cove (Figures 1 and 3). Rupture of the entire section was responsible for the 1906 **M** 7.9 San Francisco earthquake (Lawson, 1908; Brown and Wolfe, 1972; Prentice at al., 1999). The slip in the 1906 earthquake averaged 4- 5 m. Other than this large earthquake, the northern San Andreas fault has been relatively quiescent in the historical period.

An unresolved issue that bears upon the seismic hazard assessment for the northern San Andreas fault is whether the fault always or usually ruptures its full extent as in 1906, or if smaller subsections of the fault sometimes rupture coseismically, and if so, whether those subsections are long-lived, i.e. whether they constitute persistent rupture segments. In recent years, the northern San Andreas fault has been subdivided into four segments for the purpose of developing statewide seismic hazard assessments. The segments have been defined by numerous working groups (e.g. WGCEP, 1990, 2003, 2008; WGNCEP, 1996) based on ostensibly different geologic and/or rupture characteristics. This study focuses on the North Coast segment (SAN), which, as defined by the working groups, is about 136 km long and extends from the Golden Gate to Point Arena (WGNCEP, 1996; WGCEP, 2003, 2008). It is flanked to the north by the Offshore segment (SAO) and to the south by the Peninsula segment (SAP) (Figure 3). The southern end of the segment coincides with the junction of the San Gregorio fault and the San Andreas fault and also with a southward decrease in slip rate on the San Andreas fault from 24±3 mm/yr to 17± 4 mm/yr (Schwartz et al., 1998; Hall et al., 1999). The decrease in slip rate reflects the presence of the subparallel San Gregorio fault that siphons ~7 mm/yr of slip from the San Andreas fault. Slip in the 1906 earthquake also decreased south of Golden Gate from about 5 m to about 3 m. The working groups have used historical and paleoseismic characteristics to define rupture models based on these segments that include scenarios involving rupture of the full length of the fault (e.g. 1906 earthquake) and rupture of one, two, or three segments. The extent to which segment boundaries defined by geologic characteristics actually represent constraints on individual earthquake ruptures remains uncertain, but they have nevertheless formed the basis for the working groups' seismic source characterization and hazard assessment.

WGCEP (2003), and the most recent WGCEP (2008), prefer rupture models that involve failure of the entire northern San Andreas fault, as in 1906, based on similar ages for some events observed at palesoeismic sites north and south of Golden Gate, which have been inferred to be the same event. However, the timing of events is not yet well enough constrained to make such assertions with confidence, and seismic hazard models need further data that shed light on the past behavior of the fault to be more robust.

Paleoseismic data can help define the rupture length, amount of slip, and timing of past earthquakes. With well-constrained rupture ages, one can distinguish between different paleoearthquakes. Ages determined at multiple points along a fault, coupled with slip-per-event data, can in turn provide constraints on prehistoric rupture lengths (Weldon et al., 2004). Information about paleorupture extent and timing are necessary to test segmentation models with any degree of certainty. If, for example, in some prehistoric earthquakes only a fraction of the north coast section ruptured, then multiple scenarios of shorter and longer, 1906-style, ruptures need to be accommodated in seismic hazard models. If the endpoints of paleoruptures differ significantly from event to event, the entire segmentation model may be called into question.

Paleoseismic studies near Point Arena suggest a slip rate of about 16-24 mm/yr and earthquake recurrence interval from five paleoearthquakes of 200-400 yr (Prentice, 1989; Prentice et al., 2000). Prentice (1989) reported that the penultimate event occurred after AD1530 and probably after AD 1635. Slip rate investigations near Fort Ross suggest a slip rate of about 19 mm/yr (e.g. Noller et al., 1993; Noller and Lightfoot, 1997; Prentice et al., 2001;). Kelson et al. (2006)

analyzed colluvial wedge stratigraphy in trenches near Fort Ross and found evidence for four events in about 1000 years and a penultimate event at AD 1660-1812, consistent with results obtained from the nearby Archae Camp site (Noller et al., 1993; Simpson et al., 1996; Noller and Lightfoot, 1997). At Vedanta Marsh near Olema, about 45 km north of San Francisco, Niemi and Hall (1992) and Zhang et al. (2006) examined the fault where it crosses a marsh and offsets stream channels. They determined a slip rate of 24±3 mm/yr and a record of multiple paleoearthquakes with an average recurrence interval of about 250 years but with significant variability in individual interval length. The penultimate event occurred from AD 1670-1740; Zhang et al. (2006) argue that this event, if their assumption of 5m of slip in 1906 is correct, had less slip (~3m) and may have resulted from rupture of a smaller segment of the fault than the 1906 rupture. Goldfinger et al. (2008) argue that widespread turbidites deposited offshore northern California were triggered by rupture of the San Andreas fault and thus they record the occurrence of San Andreas fault ruptures. Based on this assumption, they conclude that the northern San Andreas fault has an average recurrence interval of ~200 years, the penultimate earthquake occurred in AD 1700-1750, and that most fault ruptures were longer than 250 km and may have ruptured the same extent as the 1906 earthquake. These data provide some constraints on past rupture history and the broad similarity in the ages of some paleoevents at different sites have been used to suggest simultaneous rupture; however, given the large uncertainties on the ages of past events, rupture of the fault as a series of smaller events over a short time period is equally supported by the data. Unfortunately, at this time, in spite of the paleoseismic work done to date, information on timing and rupture length adequate to determine the segmentation of the fault are still not available for the northern San Andreas Fault.

One major difficulty with developing a robust paleoseismic history for this section of the fault is that much of the fault traverses heavily forested, relatively inaccessible terrain. Air photos have failed to provide adequate detail of fault location from afar because they are images of the top of the forest canopy, not the ground, and the dense vegetation can hide all but the most well-defined geomorphic features. Field investigations to search for more subtle geomorphic features have also been hampered by difficulties in locating oneself with the same inadequate air photos, as well as in traveling through the dense vegetation. Thus, it has been challenging for researchers to map the fault precisely in this area. Certainly the kind of detailed mapping of small strands, complex zones, and subsidiary features that are necessary to understand the nature of the fault and its history has not been possible. Furthermore, it has been difficult, for the same reasons, to locate good paleoseismic sites that might yield the kind of information necessary to improve fault characterization. Thus, the northern segment of the San Andreas has lagged behind other sections that traverse more arid, less vegetated regions. However, newly developed LiDAR technology offers the possibility of enhancing remote images and improving existing mapping.

LiDAR data

The development of Airborne Laser Swath Mapping (ALSM) or LiDAR (Light Distance and Ranging) technology has provided the means to overcome some of the problems previously faced by geologists working on the northern San Andreas Fault. Because it measures multiple returns of a laser beam aimed at the ground, both the first return, from the top of the forest canopy, and the last return, from the bare earth surface, can be collected. By isolating the last returns, LiDAR is capable of revealing the land surface beneath the forest canopy even in highly vegetated areas. This technology allows geologists for the first time to undertake detailed reconnaissance geomorphic and tectonic mapping using remote imagery to identify faults scarps, displaced geomorphic features, and other tectonic landforms, and thus provide background data for undertaking site-specific field investigations.

The USGS was fortunate to obtain a suite of LiDAR surveys from northern California in September, 2003. The coverage along the San Andreas fault includes a 70-km-long swath that extends from Fort Ross in the south to Point Arena in the north that encompasses the most inaccessible, densely forested, and poorly mapped sections of the fault (Figure 2). These data were then used to create digital elevation models (DEMs) of the bare earth surface, virtually stripping the trees from land. The DEMs can have a resolution of a few meters, providing phenomenally better resolution base topography than was available from 7.5-minute topographic quadrangles. We should note, however, that the de facto resolution was variable across the surveyed area. In regions of especially dense cover and/or steep topography, the number of returns decreased considerably compared to less vegetated, less steep areas, resulting in diminished resolution. This can be seen in shaded relief images of the DEMs, where lower density of ground returns results in visible triangular facets that obscure some topographic detail (e.g. in Figure 6g, the steep slopes along the fault zone near Timber Cove Creek are heavily faceted compared to the flat, open surfaces to the west of the fault zone).

Previous Mapping

The most comprehensive mapping along the north coast section of the San Andreas prior to the acquisition of the LiDAR dataset included Lawson's (1908) field investigation of the surface rupture following the 1906 earthquake and mapping by Brown and Wolfe (1972). Lawson's work is detailed but involved spot checking at relatively accessible locations and did not include a comprehensive strip map along the full extent of the fault. Brown and Wolfe (1972) compiled such a strip map based on interpretation of aerial photographs accompanied by field checking of specific locations. Because of the dense forest cover, aerial photograph interpretation is difficult as the geomorphic features associated with the fault at the ground surface are only poorly expressed at the top of the forest canopy captured in the aerial photographs; this limited the accuracy and detail of the Brown and Wolfe mapping. In addition, the Brown and Wolfe map was compiled on 7.5-minute topographic base maps, which themselves suffer from inaccuracies in large part due to the same problems of dense forest cover and inaccessibility.

Brown and Wolfe's (1972) mapping indicates that along much of the north coast section, the San Andreas fault runs along and controls the location of Gualala and Garcia Rivers and their tributaries, a large-scale geomorphology that is evident in the aerial photographs. The major traces of the fault, often with multiple subparallel or en echelon strands, are reflected in the aerial photographs as clear but broad lineaments. Large displacements of moderate-sized streams produce distinctive offset channel morphology and large ponds underlie openings in the forest canopy, both of which features are also evident in aerial photographs. Nevertheless, finer-scale features, such as small ephemeral ponds that may have developed only in 1906 or minor stream offsets that record only one or two displacement events are generally not evident in the aerial photographs and thus were not compiled on the Brown and Wolfe (1972) maps.

The acquisition of LiDAR data has provided an opportunity to remap the fault without the limitations faced by Lawson (1908) and Brown and Wolfe (1972). Koehler et al. (2005) used the LiDAR data and DEMs to produce a new fault map of the northern San Andreas in the Gualala region, from Annapolis Rd to Voorhees Grove on the Garcia River, a 25-km long section in the middle of the surveyed extent. Their work provided a more detailed and higher resolution map of the central portion of the north coast segment that did allow them to delineate small features representing only a small number of events and also to identify possible paleoseismic sites that could yield information on the size and timing of past earthquakes. This study builds upon the work presented in Koehler et al. (2005) by providing similarly detailed mapping along most of the remaining ca 45-km of the 70-km swath covered by the 2003 LiDAR dataset.

Methods

Our mapping area was divided into three sections, northern, central, and southern (Figure 4). The northern section extended ~13 km from Oz farm on Mountain View Road southeast of Point Arena to the northern end of Koehler and others' (2005) mapping near Voorhees Grove. The central section extended ~9 km from Koehler and others' (2005) southern mapping limit near Annapolis Rd. to east of Fisk Mill Cove. The southern section extended ~13 km from the south end of the central section to Fort Ross Creek near Fort Ross.

We created hillshade images from the bare-earth DEMs to use as base maps for detailed fault mapping. The first step was a desk study to develop a preliminary digital fault map within ArcGIS, by interpreting probable fault-related geomorphology and lineaments as expressed on the hillshade images alone. We printed multiple images of the field area, including bare earth hillshades, full-feature hillshades made from DEM's of LiDAR first returns (i.e. the top of the forest canopy), preliminary fault mapping on bare earth and full-feature hillshades, and Brown and Wolfe (1972) fault mapping on bare earth hillshades. We carried out detailed field investigations, mapping onto 1:10,000-scale hard copy bare-earth hillshades. We supplemented the LiDAR-derived base maps with existing fault maps and topographic maps in the field, and used a hand-held GPS device regularly to check our locations when conditions allowed it (e.g. clearing in the forest). Finally, we modified the on screen mapping to reflect field observations and developed a final digital fault map within ArcGIS. In order to facilitate use of our maps, we chose to use the same fault trace designations and symbology that Koehler et al. (2005) used to classify the prominence and clarity of the feature including: strong evidence (solid line), distinct evidence (long dash line), weak evidence (short dash line), and concealed (dotted line).

Our field investigations were comprehensive in most of the region. We field checked the on-screen mapping by walking 27 km of the 38-km-long extent of the study area along what we interpreted to be the 1906 rupture trace. We did not field check a 9-km-long section from the southern end of Koehler and others's (2005) map to the latitude of Fisk Mill Cove because we were unable to obtain landowner permission for access to this large property (Central section, Figure 4). Our mapping in that area is based only on on-screen interpretation of the bare earth hillshade images. We also did not field check, north of the northern section, the 5 km from the coast to Mountain View Rd., or south of the southern section, the 3 km from Fort Ross Creek to the coast, because these sections are not highly vegetated and have been well mapped already using aerial photographs and topographic maps (Prentice, 1989 and Prentice, unpublished mapping). The on-screen mapping included a number of lineaments and possible fault traces that were several hundred meters from the primary 1906 rupture trace, and field checking often did not extend to examining these features. Thus, the final field-checked map may not include some distant traces that probably did not rupture in 1906. However, the GIS coverage retains the original on-screen mapping, which includes these features and is available to aid in their further investigation. That coverage also includes lineaments that we identified as possible fault traces in the on-screen mapping but which we later identified as of non-tectonic origin (e.g. roads, logging skid trails, etc). We removed these from the field-checked final map.

In addition to mapping fault traces, we also mapped and compiled within ArcGIS a database of fault-related geomorphic features, included in the final GIS as a point coverage. Although a small subset of such features was identified in our preliminary on-screen mapping, we did not identify the bulk of them until we undertook the field investigation. Many of the features were too small to identify on screen, especially in faceted areas. This was especially true of small ponds, which were ubiquitous along the length of the fault and provided some of the most common fault-related geomorphic features. Typical geomorphic features compiled in the GIS included fault scarps, with facing-direction identified, ponds, linear valleys and streams, swales and benches, offset streams, abandoned channel, and shutter ridges. Although we did not map Quaternary or Holocene deposits comprehensively, we did map scattered landslides and alluvial deposits where we considered it necessary to clarify our tectono-geomorphic interpretations. Finally, although ponds are included within our geomorphic features coverage as point features, we also created a distinct layer mapping out ponds since many ponds were laterally extensive such that point designations did not adequately illustrate them. Thus, the mapped ponds are included in the GIS as a polygon feature class, which shows their extent; the attributes of the ponds, however, are compiled in the geomorphic features coverage.

The attribute table for the geomorphic features layer in the GIS includes fields both to describe the features in some detail and to provide an abbreviated code for such features. Table 1 below shows the abbreviated codes for the compiled features; the Appendix includes a table of all the geomorphic feature sites and the contents of the detailed attribute field. Site numbers and the abbreviations are shown in the fault maps in this report (Figures 6a-h).

Table 1. Abbreviations of Geomorphic Features

Geomorphic Feature	Abbreviation
Abandoned channel	ac
Bench	b
Linear break in slope	bis
Depression	d
Drainage divide	dd
Deflected stream (distance, where noted)	ds
Fault	f
Fluvial terrace	ft
Gouge	g
Stream knickpoint	kp
Landslide	lds
Linear stream	ls
Linear valley (drainage direction, where noted)	lv (N)
No clear fault features	nff
Offset stream channel (distance, where noted)	os
Pond	p
Ponded alluvium	pa
Scarp (facing direction), height (where noted)	s (NE), 3m
Swampy ground	sg
Spring	sp
Shutter ridge	sr

Swale	sw

Results

Using the LiDAR imagery combined with field mapping, we have compiled a new strip map of the fault traces and lineaments along the 70 km stretch of the northern San Andreas Fault between Fort Ross and Point Arena that were not mapped by Koehler and others (2005) (Figure 4). The fault shows greater complexity and some marked differences with that of the best existing map, the map of Brown and Wolfe (1972), which was made using air photos, topographic maps, and field mapping. Along most of its length, the fault comprises multiple strands, albeit often with one dominant trace. In the north near Point Arena, the fault appears as two or three subparallel strands across a zone 50 to 200 m wide that parallels the Garcia River. Farther south, from Plantation to Fort Ross, it manifests commonly as a suite of closely spaced left-stepping en echelon strands. Numerous linear valleys, benches, elongate depressions, uphill-facing scarps, and ponds delineate the fault. The smallest scarps are commonly 1-2 m high and may represent only the most recent, 1906, rupture; elsewhere, larger scarps up to 30 m high, clearly reflect multiple earthquake ruptures localized along the same strand. Streams commonly flow down the steep slopes that parallel the fault zone, meet the uphill-facing scarps at right angles, and deposit young alluvial sediments at the foot of the scarps and/or are deflected to flow along the fault. Many of the ponds contain large redwood trees in growth position, now dead and with their roots deeply submerged; presumably the trees drowned subsequent to fault rupture and sudden deepening of the ponds.

In the following section, we describe the characteristics of faulting and fault-related geomorphic features along the full extent of the map area. The descriptions are organized to correspond with the eight detailed map sheets presented in Figures 6a-h. The maps are at 1:10,000 scale.

Northern Section (Garcia River)

The northern section of mapped fault includes about 13 km from Mountain View Rd. southeast of Point Arena to the northern end of Koehler and others' (2005) mapping near Voorhees Grove (Figure 5a). Geomorphic features are identified by site number in italics (e.g. (*173*)) in the text and Figure 6.

Oz farm (Figure 6a)

The northwesternmost portion of this mapping project traverses the open area southeast of Point Arena occupied by the Oz Farm and includes the northernmost extent of the Garcia River, before it turns west to head out to the Pacific Ocean. We mapped as far north as Mountain View Rd north of Oz; along the continuation of the fault to Point Arena proper the region has no forest cover and the fault has been well-mapped already with traditional methods (Prentice, 1989; unpublished mapping). The fault in the Oz region is only sporadically evident as it runs through the active Garcia River channel through much this section. On Oz farm, northwest of the sharp left bend in the Garcia River, the fault comprises several en echelon strands that come out of the northwest-trending river and cut up into the uplands. The fault is characterized primarily by broad benches and swales, with some ponds and swampy ground evident in the grassy regions near the highway (e.g. *2, 3*). Several northwest-trending linear depressions parallel the fault to the northeast, and in fact through some of their extent the fault strands occupy these depressions. Some but not all of them have been mapped as faults (Davenport, 1984) but most of them do not appear to reflect recent faulting and did not rupture in 1906 (Brown and Wolfe, 1972). They may be caused by differential erosion of underlying dipping, probably faulted, Franciscan bedrock, with some enhancement through gravitational failure; minor ground disruption has been identified on landslide maps in this area (Davenport, 1984). We consider that the most active traces of the fault are limited to the western edge of this suite of depressions. Farther southeast of Oz farm, the fault briefly reemerges from the river channel as a single strand and traverses a Holocene terrace, splits into two subparallel traces, the westernmost of which occupies a linear valley (*20-23, 25, 26*) and the easternmost of which traverses the eastern edge of a linear ridge (*27*), then drops down again onto a young alluvium as a single trace until it is concealed again by the active channel (southeast of *37*). At the northwestern end of this stretch the fault appears as a broad swale; in the linear valley, one long and numerous small ponds delineate the fault (*25, 26, 28*). The eastern strand along the ridge is expressed primarily by a west-facing scarp that is as high as 8 m (*27*).

Eureka Hill Road (Figure 6b)

In this section, the fault parallels the Garcia River along its western bank. At the northwestern end, it emerges from the active river channel and traverses a low, gravelly, Holocene river terrace (*44, 45*). The trace is not clear across this low terrace as it has probably been flooded since 1906, and the area could provide a promising site for paleoseismic investigations. To the west of the mapped trace, a steep escarpment marks the western edge of a narrow ridge. Brown and Wolfe (1972) mapped a fault trace through here. We identified numerous geomorphic features consistent with faulting – primarily swampy ground and small ponds (*39-41, 43*) – but on strike to the northwest of these features higher Holocene terraces do not appear to be faulted (*38*). An arcuate terrace riser is not visibly offset across the extension of the western ridge scarp, and it is unlikely that this terrace, which is several meters above the modern floodplain, has been modified since 1906 to the extent that it would hide evidence of 1906 rupture. Thus, we consider that although there is almost certainly a Quaternary fault in that area, it probably is not the most recently active trace. This is consistent with Lawson's (1908) descriptions of two sets of scarps, only the eastern of which ruptured in 1906; it is not clear from his description if he is describing exactly this section, but it may be.

Along the rest of this section, the fault continues as one primary trace with smaller secondary subparallel traces, and to the southeast becomes more discontinuous with subparallel and en echelon strands. Again, numerous and extensive ponds delineate the fault along much of its length; to the southeast steep, predominantly west-facing scarps as high as 15 m characterize the fault. We also observed right-laterally offset, deflected and beheaded streams (e.g. *107*) and abandoned channels (e.g. *74, 100, 101, 135*). At the southeastern end of this section, a large pond fills a depression along the fault (*129, 133, 134*). Numerous drowned trees occupy the pond, testifying to deepening and expansion of the pond since growth of the trees (Figure 7).

Lee Creek (Figure 6c)

Along this section, the fault continues to traverse the western edge of the Garcia River, and comprises one primary trace, with a few short discontinuous secondary traces. The main trace occupies linear valleys (*137, 142, 157*) and swales (*140, 147, 148, 154*) and is well defined along almost the full extent, with west-facing scarps (*143-144, 149-150, 153-154*) that are usually a few meters but reach as high as 20 m (*149*), and ponds (*140, 142-144, 146-147, 152, 155-156*) as the most common fault-related geomorphic features (Figure 8). At a latitude of about 38º53'50", a secondary trace occupies a deep linear valley east of the primary trace and west of a high ridge.

The tributary draining eastward into the Garcia River used to drain to the south of the high ridge but has been captured and now drains north, leaving the old outlet abandoned (*163*, *164*). At about 38º53’20”, another large pond (*186*) contains numerous dead redwood trees, including a large stump that was logged in the 19th century, based on the style of logging. This indicates that the pond did not occupy as extensive an area prior to 1906 and deepened and expanded following that earthquake. At the southeast end of this section, at about 38º53’00”, a short section of fault is in the active river channel. It is difficult to identify fault-related features and the active trace for about 300 m southeast of where we expect it to emerge from the active channel; the terrain here is rugged, and extensive logging with attendant road building may have obscured evidence of faulting. In the southeasternmost part of this section the fault is again well defined with two active traces.

On the western trace, located on the flanks of the west-facing scarp, a logged redwood stump (*201*) may have been offset in both the 1906 earthquake and the penultimate event. The characteristics of the sawing indicate that it was logged in the 19th century. The stump is offset both horizontally and vertically, with the flat logged top surface showing several tens of centimeters of down-to the-west vertical separation; it has also been offset right-laterally 1-2 meters (Figure 9a,b). Between the two separated pieces of stump, we can precisely match well-defined, curving “puzzle pieces” of wood; these pieces show 65 cm of sub-horizontal right-lateral displacement, with much less of a component of vertical separation than the stump itself (Figure 9b,c). In addition, the stump has been burned; most of the interior surfaces of the split stump has burned, but not the displaced puzzle pieces, suggesting the burn occurred prior to the displacement of the puzzle pieces. We interpret this stump as having possibly experienced two offset events. The earlier event split the tree but did not kill it or completely break it in two throughout; rather it continued to grow with a split basal trunk. In the 19th century, the tree was cut down, with each piece of trunk individually logged. The two people required to saw the trunk by hand would have stood at the same level relative to the base of the tree while cutting each part. Since the tree was growing on a scarp, the east part was on higher ground than the lower, so the upper sawn surface was thus probably also higher on the eastern trunk. Then, in 1906, the now logged stump was again offset, with about 65 cm of horizontal and negligible vertical displacement. This scenario accounts for the mismatch in displacement between the stumps and the puzzle pieces and explains the greater component of vertical separation of the stumps’ logged surfaces. Further study of this stump could provide information on the timing of the penultimate event.

Iverson Road (Figure 6d)

Throughout this section the fault comprises two or three traces. Along most of their extent, all traces occupy narrow linear valleys flanked by west-facing scarps (Figure 10). The fault is not evident as it crosses a steep canyon at about 38º52’30” but is otherwise well defined until it enters and occupies a deep active drainage that has captured the outflow of several tributary streams. This drainage marks the end of our southern section and the boundary between the mapping areas of this study and Koehler and others (2005). This section also includes one large pond (*272, 276*) containing numerous drowned redwood trees in growth position. The outlet of this pond is presently at the east side of the pond about half way along its extent (*274*). The water exits through a broad shallow gap in a west-facing scarp, and flows without a defined across the road; at the far end of the road, the water flows out a defined channel. A few meters south of the outflow, bedrock is exposed in the road; if bedrock floors the outflow as well, there may be no well-defined channelization of pond drainage established between earthquakes. At the south end of the pond, a road runs along the top of the scarp that flanks the eastern edge of the pond. This road, which may be built up somewhat from the natural scarp, was about 3-4 m above the water level in the pond in July 2005. To the east side of the road, a now abandoned channel (*282*) represent a former outflow channel for the pond; the channel was about 2 m below the top of the road in 2005 and thus about 2 m above the water level of the pond.

Southern Section

The southern section of our mapping includes about 24 km of fault from about latitude 38º36'30" to Fort Ross Creek near Fort Ross (Figure 5b).

Plantation (Figure 6e)
In the northwestern part of this section, the fault comprises multiple left-stepping en echelon traces; in the southeastern part, it comprises two subparallel strands. The fault zone is west of and parallel to a linear tributary to the South Fork of the Gualala River; the tributary is itself fault controlled, though the most recent faulting does not appear to occur within it. In the northwestern part, the outer traces area characterized by low (1-4m), predominantly west-facing scarps (e.g. *298, 300, 302, 309, 311, 312, 315, 342, 344*), small linear valleys (*298, 300-302, 309, 346, 350*), swales (*299, 305, 339*), and small ponds (*344, 346, 350*). The inner traces occupy deeper, more well-defined linear valleys flanked by larger scarps as high as 10 m (*327*; Figure 11), suggesting these traces may have carried a larger proportion of the slip than the outer traces; they are on strike with the two traces that continue to the southeast. At latitude 38º36'30", a tributary to the linear tributary described above used to flow along the northern part of the western of the central strands before emerging at a right angle and flowing out to the tributary. This outflow channel has been abandoned and this tributary now flows directly into the South Fork of the Gualala River (just north of *298*). The westernmost of the en echelon traces also controls the flow of several small streams which have been deflected along them. Where the streams flow into the scarp, alluvium has ponded behind the scarp (*307, 313*). Lower Lake, the small lake located at the southern end of the en echelon traces used to flow out a channel at its southern end that has since been abandoned (353); it now drains to the north along the east-central trace (*338*). South of this lake, the fault traverses land of Plantation farm and camp as two subparallel traces. The western trace passes along the western edge of and through Lake Oliver; the eastern traces passes through forest and meadow east of the lake. Lawson (1908) describes the 1906 rupture as traversing Lake Oliver and the passing through the farm buildings and pasture of Plantation farm as a 270-ft-wide zone comprising six distinct traces, but we found no evidence of this in the pastures south of the house and the road that crosses the property (*369*). The eastern strand, however, remains clear through this section. At the southern end, immediately north of the road, the fault has split and offset a tree (*370*; Figure 12). South of the road and a deep stream channel in which the fault is not evident, the western trace is again visible and occupies a narrow linear valley (*371*) with an elongate pond (*375*). The eastern trace passes along gentle ground and is delineated by benches (*372, 376, 379, 381, 382, 385, 386*) and swampy ground (*379, 381*).

Salt Point State Park (Figure 6f)
In this section, the fault passes through Salt Point State Park. In the northwestern part, the fault comprises three traces characterized by predominantly east-facing scarps, 1-4 m high (*387-391, 411-412, 417, 427*), benches (*385-386, 391, 398, 408, 414, 416, 420*), and swales (*397, 399-401,*

406, 411, 419, 422, 424, 431). North of the access road that descends from Seaview Road (road meets the fault zone at about *426*), the multiple closely-spaced traces are marked by numerous small ponds and patches of swampy ground and occupy short linear valleys and broader benches and swales (*397-426*). South of the road, we were unable to identify continuations of several of the traces from the north, and we have mapped one primary trace that traverses the foot of the steep slopes west of Seaview Road and east of a large pond/lake (*429*). The vegetation was dense and low in this area, however, and travel was difficult, so we cannot rule out having missed some features and traces in this section. The fault continues as one primary trace, with low east-facing scarps (*441, 442, 446, 460, 462-463, 465-468, 472*), to near the southeastern end of this section where it becomes more complex, as described below.

Timber Cove Road (Figure 6g)
The fault in this section is characterized by multiple, short, discontinuous, en echelon traces occupying a zone about 100-200 m wide. At the northwestern end, the fault zone comprises as many as five strands, with ponds of various sizes occurring along most of them, some containing drowned trees and logged stumps (*483, 485, 493, 497*). Scarps are primarily east facing and 3-4 m high (*476, 487, 496, 497, 499, 500*), although in places they reach 8 m (*491*). From about latitude 38º33’30” to where Timber Cove Road. crosses the fault, the fault is difficult to identify through a 400-km-long stretch of large, deflected and modified drainages; few distinct fault features are evident and traces cannot be followed for a significant distance. South of Timber Cove Road, the fault again appears clearly as a zone with multiple en echelon strands. Most of the traces are well defined, but the geomorphic expression is somewhat more subdued than in some other regions to the north, with the location of the fault indicated more commonly by benches and swales (most sites between *525* and *600*) than deeply incised linear valleys and streams (*540, 551, 557, 56, 562, 566, 568, 572, 584, 590, 597*). The active fault zone traverses the east bank of the prominent right-lateral offset of Timber Cove Creek. To the south of this stream, the fault zone narrows and a single strand with a well-defined west-facing scarp (*610-614*) dominates as the fault approaches the broad open meadows of Buttermore Ranch (Figure 13). At Buttermore Ranch, Lawson (1908) describes three rupture traces, the primary of which is probably that located along the large west-facing scarp.

Fort Ross (Figure 6h)
The southernmost mapped section extends from Buttermore Ranch to Fort Ross Creek. The northwestern half of this section, from Buttermore Ranch to the large right-laterally offset Kolmer Gulch, the fault is poorly expressed. The fault occupies steep-sloped, deeply incised valleys and active streams. The steep flanking slopes are prone to gravitational failure, and the numerous landslides and debris flows in this region obscure the fault and related geomorphic features. South of Kolmer Gulch, the fault traverses the steep slopes east of the stream jog as numerous short, discontinuous subparallel strands occupying gentle swales (*630, 631, 633*) and broad benches (*632-634, 638, 640-641, 644*) and sometimes more sharply defined linear valleys (*635, 636, 639*); a few small ponds occur along the fault (*635*). Near Fort Ross Rd, the fault emerges from the forest and traverses cleared meadow land. Multiple traces occupy extensive swales with intermittent ponding (*645-647, 649-651, 653-656, 660, 661, 668, 670*). Near Fort Ross Rd., numerous trees have clearly been topped, having lost their upper reaches during the 1906 earthquake (*657 and west*; Figure 14). The fault is well-expressed across the open meadowland, but becomes obscure again near Fort Ross Creek where steep slopes of the

drainage have been extensively affected by landslides. We ended our mapping at this creek, since the fault has been well mapped to the south (Prentice, 1989; C. Prentice, pers. comm.).

Central Section

A 9-km-long section of fault between the northern end of our southern section and the southern end of Koehler and others' (2005) mapping constitutes our central section and is owned by members of a single family (Figures 4 and15). We mapped the fault in this region on screen based on lineaments and fault-related features expressed in the LiDAR imagery, as we did as a first step for the other sections. We were unable, however, to obtain permission from the landowners to enter the property for field checking purposes. The mapping here, shown at 1:30,000 scale in Figure 15, is entirely based on in-office interpretation of LiDAR imagery. We found, in the course of this investigation, that a number of features identified in the LiDAR as possible fault-related lineaments in fact turned out to be non-tectonic (e.g. roads, logging skid trails, etc.) when we field-checked them. Consequently, the mapping in this central section may include lineaments of non-tectonic origin and older, now inactive, faults as well as the most recent traces.

Paleoseismic Sites

One of the primary concerns in assessing the hazard posed by the northern San Andreas fault, or indeed any fault, is establishing the extent of likely fault ruptures as well as the magnitude of single event displacement. Paleoseismic data can provide constraints on these parameters if well-developed event chronologies, especially if combined with single-event displacement information, are obtained at multiple sites along a fault. Consistent event chronologies at adjacent sites support, though do not prove, throughgoing ruptures, whereas clearly different chronologies, if accurate, preclude throughgoing rupture. Current hazard models put heavy weight on 1906 rupture characteristics for the northern San Andreas fault; developing event chronologies at sites along the north coast section can help determine if such weight is justified. To date, no paleoseismic data exist between Alder Creek and Fort Ross, so identifying potential sites is an important aspect of fault mapping in this region.

The fault is well defined through most of the mapped extent, and the plethora of uphill-facing scarps and small, seasonal ponds provide possible locations for paleoseismic investigations. Unfortunately, the steep slopes, extremely dense vegetation and lack of throughgoing roads make access difficult to near impossible for many of the potential sites. Nevertheless, we have identified a few locations where detailed study could shed light on this heretofore lightly studied portion of the San Andreas fault.

One promising site (*467*) is located on Salt Point State Park land at about latitude 38º34'00". The fault is in one primary traces here; a second en echelon trace is evident just to the south, and there are two short, questionable lineaments to the west, but this strand probably has been carrying most of the slip. The fault emerges from a linear valley into a broad open area. The fault here is marked by a small east-facing scarp, which is partially buried in alluvium that has been deposited against the scarp (Figure 16). The alluvium is young and clearly buries the base of the trees that grow within the fan to the east of the scarp, suggesting a relatively high sedimentation rate. The fan material exposed at the surface comprises pebble to small cobble gravel and sand, which should provide well-stratified deposits appropriate for interpreting stratigraphic and faulting relationships in a trench. Just south of the site, a deeply incised northwest-trending channel is headwardly eroding and draining the trench area, so it is less likely that one would encounter water at very shallow levels in a trench.

Summary and Conclusions

The research presented here reflects the advances that can be made by combining state-of-the-art remote sensing imagery and high-resolution topographic data with traditional field mapping. We have compiled a new strip map along about 38 km of northern San Andreas fault between Point Arena and Fort Ross that incorporates information obtained from high-resolution LiDAR surveys that provide detailed georeferenced images and topographic data of the ground surface beneath a dense forest canopy as well as from detailed field mapping involving walking almost the entire length of the mapped fault. This new mapping refines existing mapping of Brown and Wolfe (1972) that was developed using traditional imagery and topographic data such as aerial photographs and 7.5-minute topographic quadrangle maps supplemented by reconnaissance mapping and spot checking. In places the fault zone had been mislocated by up to several hundred meters because of the difficulty of identifying clear lineaments in the forested terrain. In addition, this new mapping indicates that the fault zone has greater complexity overall than was revealed in Brown and Wolfe's (1972) map. We hope our map represents a significant improvement on existing mapping and will help researchers with more detailed investigations of the earthquake geology of the northern San Andreas fault.

LiDAR data have been crucial in identifying lineaments that may be fault traces or fault-related features. Topographic detail well beyond what is possible with air photos is available, and scarps, swales, linear valleys and other fault-related features with a distinct topographic signature are evident in the imagery. LiDAR data also allow better preliminary mapping of a wider area than is possible with air photos or topographic maps; improved mapping speed in densely forested terrain because of the better preliminary map and because less time is wasted in locating oneself; topographic profiling in the office without extra equipment or field time. We encountered some problems with this particular LiDAR dataset, specifically the occurrence of pronounced faceting in the DEMs in some locations. This occurs in places where conditions such as very dense forest cover or steep relief inhibit full penetration of the laser pulses, such that the last recorded return doesn't reach the ground; the "bare earth" data thus include fewer points. When the data points are linked in a TIN (triangulated irregular network) to create the bare-earth DEM, the widely spaced data yield large triangular facets in the image (e.g. along the big stream channel in the center of Figure 6h). In faceted areas, facets can line up to create apparent lineaments that are, in fact, spurious.

Mapping in the office using LiDAR topographic data and imagery does not replace field work for mapping faults but complements and enhances it and makes it easier. In fact, one conclusion we have drawn from this and the related field research is that, even with the incredibly improved imagery available with LiDAR, we cannot dispense with field work; it remains the backbone of fault mapping. The field work we undertook generated significant changes from the onscreen mapping and contributed to a greatly improved final map. Specifically, the LiDAR did not always reveal fault-related features that do not have a distinct topographic signature; for example, shallow, ephemeral sag ponds, very common and distinctive fault-related features in this area, were generally not visible on LiDAR. In the field, however, we were able to locate and characterize numerous geomorphic features, such as sag ponds, small uphill facing scarps, ponded alluvium and minor offset streams that were too small to identify in the LiDAR data. Some of these limitations could be removed with higher-resolution LiDAR. A cursory comparison of the LiDAR data we used for this project with new higher-resolution data obtained along the fault in 2007 and available in spring 2008 indicates that the new data provides DEMs with greater detail than our dataset and specifically has largely dispensed with the faceting problem we faced. This could allow identification in the imagery of some of the smaller features we were only able to identify in the field, although the time to dispense with field work entirely has still not arrived.

The development of an improved, high-resolution strip map along the fault is not the last step in fault investigations on the northern San Andreas but rather one of the first. This section of fault remains poorly understood, and seismic hazard models to date are based on few data and are strongly model driven. One of the key elements in assessing the seismic hazard posed by a fault is the likely extent of future ruptures and the possible existence or non-existence of long-lived rupture segments. Current models that identify distinct segments and that favor repetition of 1906 events are possible but not constrained by paleoseismic data. Such data, specifically information on the ages of paleoearthquakes at multiple locations along the fault and the size of prehistoric ruptures, are necessary to assess whether current models best characterize the fault's behavior. To date, paleoseismic sites are few and far between, and cannot yet provide answers to these questions. Specifically, there have been no paleoseismic sites between Fort Ross (Kelson et al., 2006) and Point Arena (Baldwin, 1996; Baldwin et al., 2000; Prentice et al., 2000), approximately the entire extent of this study area. Although the inaccessibility and dense vegetation in this region limit the number of possible paleoseismic sites, nevertheless, we have now identified a few promising sites and hope the new map will facilitate other researchers in identifying and investigating further locations. Those investigations could yield the results necessary to refine hazard models of the northern San Andreas fault.

Non-technical Summary

We have used LiDAR (Light Distance and Ranging, also known as Airborne Laser Swath Mapping [ALSM]) imagery from coastal California between Fort Ross and Point Arena to create a map of the northern San Andreas fault. LiDAR technology uses lasers to penetrate the dense redwood forest canopy, and the data yield a detailed terrain model of the ground surface. We have thus been able to see fault-related geomorphic features in unprecedented detail and consequently produce an improved strip map of the most recently active traces of the fault. This map is necessary to further detailed studies of the fault that shed light on the fault's earthquake history and hazard.

Acknowledgments

This research was funded by the U.S. Geological Survey's National Earthquake Hazards Reduction Program (Award # 05HQGR0069). We thank Mendocino Redwoods Company and more private landowners than we can mention for allowing us access to their property.

References

Argus, D., and Gordon, R., 2001, Present tectonic motion across the Coast Ranges and San Andreas fault system in central California, Geol. Soc. Am. Bull. v. 113, p. 1580–1592.

Baldwin, J.N., 1996, Paleoseismic investigation of the San Andreas fault on the north coast segment, near Manchester, California: M.S. thesis San Jose State University, 127, p. plus plates.

Baldwin, J.N., Knudsen, K.L., Lee, A., Prentice, C.S. and Gross, R., 2000, Preliminary estimate of coseismic displacement of the penultimate earthquake on the northern San Andreas fault, Pt. Arena, California, in Proceedings of the 3rd conference on Tectonic Problems of the San Andreas Fault System, Bokelmann, G. and Kovach, R.L. eds, Stanford University, Stanford, California.

Brown, R.D., Jr., and Wolfe, E.W., 1972, Map showing recently active breaks along the San Andreas fault between Point Delgada and Bolinas Bay, California: U.S. Geological Survey Miscellaneous Geologic Investigations Map I-692, scale 1:24,000, 2 sheets.

Davenport, C.W., 1984, Geology and geomorphic features related to landsliding, Point Arena NE (Eureka Hill) 7.5´ Quadrangle, Mendocino County, California, California Division of Mines and Geology Open-File Report 84-47, scale 1:24,000.

Goldfinger, C., Grijalva, K., Bürgmann, R., Morey, A.E., Johnson, J.E., Nelson, C.H., Gutiérrez-Pastor, J., Ericsson, A., Karabanov, E., Chaytor, J.D., Patton, J., and Gràcia, E., 2008, Late Holocene Rupture of the Northern San Andreas Fault and Possible Stress Linkage to the Cascadia Subduction Zone, Bulletin of the Seismological Society of America, Vol. 98, No. 2, pp. 861–889, April 2008, doi: 10.1785/0120060411.

Hall, N.T., Wright, R.H., and Clahan, K.B., 1999, Paleoseismic studies of the San Francisco Peninsula segment of the San Andreas fault zone near Woodside, California: Journal of Geophysical Research, v. 104, no. B10, p. 23,215-23,236.

Kelson, K.I., Streig, A.R., Koehler, R.D. and Kang, K.-H., 2006, Timing of Late Holocene Paleoearthquakes on the Northern San Andreas Fault at the Fort Ross Orchard Site, Sonoma County, California, Bulletin of the Seismological Society of America, Vol. 96, No. 3, pp. 1012–1028, June 2006, doi: 10.1785/0120050123.

Koehler R.D., Baldwin, J.N., Prentice, C.S., Pearce, J.P, 20054, Holocene geologic characterization of the northern San Andreas fault, Gualala, California, National Earthquake Hazards Reduction Program Final Technical Report, NEHRP External Grant Award Number 03HQGR0045, http://www.earthquake.usgs.gov/research/external/research.php

Lawson, A.C., chairman, 1908, the California earthquake of April 18, 1906: Report of the State Earthquake Investigation Commission (Reprinted 1969), v. 1,m Carnegie Institution of Washington Publication, 451 p. and atlas.

Niemi, T.M. and Hall, N.T., 1992, Late Holocene slip rate and recurrence of great earthquakes on the San Andreas fault in northern California: Geology, v. 20, p. 195-198.

Noller, J.S., and Lightfoot, K.G., 1997, an archaeoseismic approach and method for the study of active strike-slip faults: Geoarchaeology: An International Journal, v. 12, p. 117-135.

Noller, J.S., Kelson, K.I., Lettis, W.R., Wickens, D.A., Simpson, G.D., Lightfoot, K., Wake, T., 1993, Preliminary characterizations of Holocene activity on the San Andreas fault based on offset archaeologic sites, Fort Ross State Historic park, California: U.S. Geological Survey, National Earthquake Hazards Reduction Program, Final Technical Report.

Prentice, C.S., 1989, Earthquake geology of the northern San Andreas fault near Point Arena, California: California Institute of Technology, Pasadena, California, PhD Dissertation, 252p.

Prentice, C.S., Merritts, d.J., Beutner, E.C., Bodin, P., Schill, A., and Muller, J.R., 1999, Northern San Andreas fault near Shelter Cove, California: Geological Society of America Bulletin, v. 111, no. 4, p. 512-523.

Prentice, C.S., Langridge, R., Merritts, D.J., 2000, Paleoseismic and Quaternary Tectonic Studies of the San Andreas Fault from Shelter Cove to Fort Ross, Paleoseismic and Quaternary tectonic studies of the San Andreas fault from Shelter Cove to Fort Ross [abs.], in Bokelmann, G., and Kovach, R.L., ed., Proceedings of the Third Conference on Tectonic Problems of the San Andreas System: Palo Alto, California, Stanford University Publications, p. 249-350.

Prentice, C. S., Prescott, W.H., Langridge, R., and Dawson, T., 2001, New geologic and geodetic slip rate estimates on the North Coast San Andreas fault: approaching agreement?, Seismological Research Letters, v. 72, p. 282

Schwartz, D.P., Pantosti, D., Okumura, K., Powers, T.J., and Hamilton, J.C., 1998, Paleoseismic investigations in the Santa Cruz Mountains, California: Implications for recurrence of large magnitude earthquakes on the San Andreas fault: Journal of Geophysical Research, v. 103, p.17,985-18,001.

Simpson, G.D., Noller, J.S., Kelson, K.I., and Lettis, W.R., 1996, Logs of trenches across the San Andreas fault, Archae Camp, Fort Ross State Historic Park, Northern California: U.S. Geological Survey, National Earthquake Hazards Reduction Program, Final Technical Report.

U.S. Geological Survey and California Geological Survey (USGS/CGS), 2006, Quaternary fault and fold database for the United States, accessed 6/27/07, from USGS web site: http//earthquakes.usgs.gov/regional/qfaults/.

Weldon II, R. J., K. Scharer, T. Fumal, and G. Biasi (2004). Wrightwood and the earthquake cycle: what a long recurrence record tells us about how faults work, GSA Today, 14(9), 4-10.

Working Group on California Earthquake Probabilities (WGCEP), 1990, Probabilities of large earthquakes in the San Francisco Bay region, California: U.S. Geological Survey Circ. 1053, 51 p.

Working Group on California Earthquake Probabilities (WGCEP), 2003, Earthquake Probabilities in the San Francisco Bay Region: 2002–2031, USGS Open-File Report 2003-214.

Working Group on California Earthquake Probabilities (WGCEP), 2008, The Uniform California Earthquake Rupture Forecast, Version 2 (UCERF 2), USGS Open File Report 2007-1437, CGS Special Report 203, SCEC Contribution #1138, Version 1.0.

Working Group on Northern California Earthquake Potential (WGNCEP), 1996, Database of Potential Sources For Earthquakes Larger than Magnitude 6 in Northern California, U.S. Geological Survey Open-File Report 96-705.

Zhang, H., Niemi, T., and Fumal T., 2006, A 3000-year record of earthquakes on the northern San Andreas fault at the Vedanta marsh site, Olema, California: Seismological Research Letters, v. 77, p. 176.

Reports published

None to date. Publication of a GIS of the fault map along the entire LiDAR coverage area, including both the results of this study and those of Koehler and others (2005), is in preparation.

Data availability

The LiDAR data are available at http://core2.gsfc.nasa.gov/LiDAR/. The GIS shapefiles for this mapping can be obtained by contacting Carol Prentice or Judith Zachariasen. The limitations of the online reporting of the External Grants program required that we decrease the resolution of the map figures. For higher resolution PDFs of the figures please contact Judith Zachariasen.

Appendix

Table 1.

Site	Feature Description
1	linear valley; west faicng scarp
2	pond
3	swale
4	bench; scarp, west-facing
5	swampy ground
6	no stream deflection
7	west-facing scarp
8	bench; scarp west-facing
9	west-facing scarp; bench; swale
10	bench; scarp, west-facing
11	scarp, east-facing
12	swale; small scarp, east-facing to 1 m
13	swale
14	bench; SE of here, prominent swale behind first ridge E of river
15	swale
16	swale (N35W); high ridge between here and river
17	very steep west-facing scarp; bench/terrace above and below
18	bench to E of swale
19	bench; scarp, west-facing
20	swale with ponded alluvium against west-facing scarp
21	subtle swale
22	west-facing scarp; dies to NW
23	scarp, west-facing; alluvium panding agaisnt scarp
24	swale across ridge, N15W
25	pond, ca 200m long to south; pond from here to CP 5-3; eastern trace less distinct than to S
26	pond pinches closed, scarp eroding back
27	shutter ridge, west-facing scarp to 8m
28	pond (from here north ca 200 m); scarp. west-facing; 50 m east is small swale, trace
29	pond, west-facing scarp
30	ponded alluvium; good trench site except for access
31	west-facing scarp blocking pond
32	scarp from slump within west-facing scarp ridge
33	bench; N35W; could be old road, probably bench first
34	bench, swale
35	small marshy areea
36	swale, scarp, west-facing, small
37	bench
38	no clear scarp across terraces; no displacement of risers
39	swampy ground
40	pond; swampy ground
41	pond; ridge has rounded pebbles and cobbles
42	no fault features evident
43	pond; swampy ground; no sharp features - old fault?
44	scarp, east-facing, very subtle; possible trench site
45	subtle scarp, east-facing
46	bench
47	bench
48	bench
49	small pond
50	houses on flat; to swales on flat E of main house
51	swale; N35W
52	bench; trace less well-defined than trace to W
53	swale
54	swale
55	pond, small
56	poorly defined swale
57	swale
58	scarp, east-facing
59	scarp, east-facing, poorly-defined
60	dry swale; to E stream diverges from fault; east-facing scarp and bench continue NW to houses
61	linear stream; scarp, east-facing; bench
62	NW end of long pond; west-facing scarp; 20 m E linear valley w/ rd parallel to fault - trace?
63	scarp
64	northeast-facing scarp, 3m
65	scarp, east facing 12 m
66	south end of pond noted to northwest
67	scarp, west-facing, >6m
68	swale
69	scarp, to 12 m; linear gully along base
70	scarp, 6 m; alluvial surface?, trench site?
71	scarp, west-facing, low
72	pond; possible trace south of here near shed and orchard
73	scarp to 10 m, long pond in linear valley
74	abandonned channel
75	active channel, maybe modified?
76	alluvium pnded against scarp; altered drainage to drain swamp?
77	swampy meadow, artificially drained
78	swale; pond, seasonal
79	pond
80	fault meets road on N end; no fault features to S

Site	Feature Description
81	break in slope E of rd; fault in rd; west-facing scarp 10m W of steep slope to river
82	scarp modified by log landing and road
83	broad, subtle bench
84	weakly defined broad ridge
85	scarp, west facing, 3-4 m, swale to S; fault out of river to N
86	no fault features
87	scarp, west facing; swampy ground
88	road, no fault features
89	west-facing scarp; road along scarp
90	west-facing scarp, swampy ground; road just west of fault
91	springs; feature less well defined
92	scarp, west-facing; swampy ground
93	west-facing scarp; swampy ground
94	fault poorly expressed
95	fault less distinct into canyon to south
96	fault bends into canyon
97	linear stream coincident with fault
98	no obvious fault features south to abandonned channel
99	bench with road; low west-facing scarp - natural?
100	abandonned outlet
101	abandonned channel, now flowing north
102	pond, 20-30 m, N20W; scarp, west facing, 2 m
103	east-facing scarp
104	linear valley to SE; pond to SE; no fault features north across channel
105	subtle right bend in stream; no scarp
106	long pond
107	offset stream, RL; scarp, west facing disturbed by road; less distinct than E trace
108	pond pinches to a few m wide
109	bench, swale
110	scarp, west facing, sometimes in road; southern end of this trace
111	S end of long pond
112	outlet channel for pond to south; swampy ground to SE
113	swampy ground; canyon to SE drains out here; west-facing scarp
114	ponded alluvium; swampy ground; drains N: poss trench site but drain cut on sc
115	pond
116	abandonned channel
117	abandonned channel, former outlet for pond to S?; N end of pond; swale
118	pond; scarp, west facing to 15 m
119	scarp, west facing, 2 m
120	north end of long pond; scarp, west facing to 8 m
121	pond; west-facing scarp to 8 m

Site	Feature Description
122	pond (continues to SE); west-facing scarp to 12 m
123	scarp, west facing to 15 m; S end of pond
124	west-facing scarp to 15m
125	pond; scarp, west facing to 12 m
126	drainage does not go through scarp
127	broad swale; small seasonal pond; swampy ground
128	scarp, east facing along road
129	N end of pond, outlet
130	knickpoint
131	scarp, west facing; bench to swale to N
132	swale
133	scarp, west facing to 8 m; pond 30 m wide
134	pond, south end; dead trees, stumps in pond; low scarp, west facing to 1.5 m
135	abandonned channel, N85W
136	swale
137	linear stream along fault
138	broad swale, indistinct
139	outlet for pond to creek to N
140	pond; swale
141	stream drains north
142	small pond to NW; linear drainage
143	pond; west-facing scarp ~10m
144	scarp, west facing; pond
145	abandonned channel; road crosses fault through gap in ridge
146	north end of elongate pond, continues to southeast; west-facing scarp
147	southeast end of elongate pond; west facing scarp to north changes to swale
148	swale; swampy ground
149	steep scarp, west facing, to 20 m
150	scarp, west facing, 2 m
151	small scarp, east facing
152	pond, 6-8 m wide
153	scarp, west facing to 8 m
154	broad swale; 2 m scarp, west facing; abandonned channel to east
155	pond
156	pond
157	linear valley
158	west-facing scarp, ca 5m
159	road, no obvious fault features
160	abandonned channel, flows out N ch now, S ch too at high flow; ponded alluvium
161	bench, west of road
162	swale; scarp, west facing
163	current channel, stream capture
164	abandonned channel
165	linear valley, here south
166	scarp, west-facing, swale

Site	Feature Description
167	linear valley, drains SE, west-facing scarp to 3m
168	linear valley, pond, west-facing scarp NW of road
169	broad (20 m wide) swale, scarp, west facing to 4 m
170	linear valley, drains NW
171	linear valley, draining SE
172	linear valley
173	linear valley, east-facing scarp
174	pond filled with logs, in linear valley w/ west facing scarp to 3m
175	scarp, west facing, linear valley to north
176	swampy ground, depression
177	fault along road
178	scarp, west facing to 4 m; offset stream right lateral with vertical step
179	fault in road, from stream south to next drainage
180	swale
181	broad swale w/ low west-facing scarp; stream drains north along fault
182	head of linear valley to south
183	linear valley drain to SE, west-facing scarp
184	broad valley, fault location uncertain
185	flat-floored valley 8 m wide; scarp, west facing to 4 m
186	pond, wide, deep, w/ dead redwoods including logged stump
187	deep linear valley, drains south; fault east of road; offset stream
188	bench, east and 3 m down from road; fault diverges from valley
189	bench to swale, broad
190	swale
191	pond
192	pond narrows; linear valley to south against west facing scarp to 6 m
193	S end of pond; berm btwn pond & canyon edge; now drain N, if ponds full would top berm, drain S
194	no fault features
195	swampy ground, no obvious fault features
196	no fault features
197	swale, prob abandonned channel; road
198	bench; fluvial terrace; road
199	ponded alluviium
200	broad swale
201	linear valley, flat-floored with standing water; offset stump, RL and V (65 cm most recent)
202	high flow channel; bedrock west, alluvial gravel eas
203	ponded alluvium; deflected stream > 8m; can't follow fault north
204	no fault features
205	broad swale, ponded alluvium from two drainages, scarp, west facing 4-5 m

Site	Feature Description
206	fluvial terrace
207	linear valley draining southeast, point at head
208	road
209	scarp, west facing; north end of pond
210	scarp, west facing
211	linear valley; swampy ground; road crosses fault; stream through culver
212	pond
213	scarp, west facing to 6 m
214	scarp, west facing; pond
215	linear valley drainsN; scarp, west facing
216	swampy ground
217	linear valley
218	offset stream; scarp, west facing
219	linear stream drains southeast
220	linear valley daining north; parallel to and E of road
221	linear valley with ponded alluvium and swampy ground
222	road crosses fault
223	linear valley N20W; steep to N. flat to S
224	flat-floored valley with small ponds
225	linear stream
226	linear valley draining SE; scarp, west facing
227	linear stream drains south
228	fault in road (N20W)?
229	straight narrow linear valley here north to CP 1a-16; point is at head of gully
230	fault crosses road
231	linear valley here to south
232	no fault features; steep canyon
233	road
234	linear valley draining southeast
235	bench
236	ponded alluvium with spring; linear valley
237	scarp, west facing
238	steep linear valley draining north
239	swale; road diverges from fault
240	scarp, west facing, crosses road
241	scarp N25W. west facing, swale with road
242	linear stream, swampy ground
243	scarp, west facing; linear valley; swampy ground
244	broad swale 20 m wide; scarp, west facing,height decreases south; ponding to south
245	pond, swampy ground to north; linear valley to south
246	bench to swale, wide
247	no fault features evident, could be in road
248	fault crosses road
249	wide bench
250	landslide head scarp, west facing

Site	Feature Description
251	scarp, west facing
252	linear valley with stream
253	linear valley; fault diverges from stream and rejoins 20 m north
254	linear valley, with stream flowing north; scarp, west facing
255	stream capture left-laterally, drains linear valley from south to north from CP 0-40 to CP 0-41
256	fault unclear, in stream?
257	broad swale to linear valley, west-facing scarp, poorly-defined
258	linear valley
259	narrow linear valley with sparse ponding to south
260	swale in road
261	bench, below road
262	fault crosses rd; linear valley; steep west-facing scarp (N30W); to NW steep linear stream
263	bench, along road
264	pond; scarp, west facing; linear valley with ponding
265	drainage divide, linear valley to north drains north; fault intersects road
266	linear valley turning to bench north, along road
267	linear valley
268	linear valley, scarp west facing
269	linear valley 20 m wide, narrows northward; N35W
270	scarp, west facing, pond to swampy ground
271	scarp, west facing; linear valley
272	pond, drowned redwoods and live trees in pond; extends about 200 m
273	pond outlet; flow across road; bedrock in rd S of outlet; outlet at deeper infilled channel?
274	swampy ground
275	scarp, 1.5 m, modified by road
276	pond, with many dead trees; recently created? 1906? possibly 2 generations trees
277	springs in road at gully head
278	headward erosion, big gully, landslide
279	fault obscured by road
280	road cut, fault to west at pond edge
281	bench
282	abandoned channel, drainage 3-4 m higher than pond level
283	scarp, east facing, increasing height northward
284	scarp, west facing
285	pond, scarp, west facing
286	no ff from here to CP 0-10 to NE
287	spring in linear valley, scarp, west facing, increases north to 3 m, swampy ground
288	no evidence of fault features
289	swampy ground
290	linear valley draining pond to north

Site	Feature Description
291	fault features not evident; fault in canyon or along road
292	no fault features on traverse SW from here
293	scarp, west facing, low
294	abandoned channel, modified by road cut; fault west of here
295	bench (weak)
296	ill defined bench here NW to CP0-17; no distinct fault features
297	rd, not fault feature
298	linear valley; scarp, west-facing, to 4 m
299	swale
300	west-facing scarp; linear valley drains north steeply; sharp ridge to east
301	linear valley
302	lv to northwest; scarp, west-facing, to 4 m
303	steep, narrow linear stream
304	abandonned channel
305	swale
306	no fault features from here southeast to eastern strand south of drainage
307	ponded alluvium
308	abrupt change from linear stream to north, broad valley to south
309	subdued scarp, west-facing; linear valley
310	drains to northwest
311	subdued scarp, west-facing, to 1m
312	scarp, west-facing; broad swale; drainage to north
313	ponded alluvium
314	linear stream from here south
315	low scarp, west-facing
316	linear valley from here south, with change in trend; fault not distinct to north
317	swampy ground
318	linear valley
319	road; no fault features; GPS point
320	linear valley drains north; small pond in valley
321	linear valley draining to north; west-facing scarp, height decreasing to north
322	pond continues to south; steep west-facing scarp
323	pond, separated from pond to south by small dry area
324	pond with grass
325	broad linear valley to swale; scarp, west-facing, decreases in height to north
326	deep, steep linear canyon, brushy
327	strands merge; scarp, west-facing, to 10 m; linear valley
328	linear valley; scarp, steep, west-facing
329	scarp, southwest-facing to 3m; pond to north
330	pond; scarp, west-facing
331	scarp, southwest-facing on east side of pond, to 2 m

Site	Feature Description
332	fault poorly defined
333	abandonned channel head for east-draining channel; now along fault
334	linear valley (N30W); west-facing scarp; pond (dry)
335	linear stream (dry)
336	linear valley
337	linear valley with ponding to linear stream
338	scarp, west-facing; lake outlet
339	broad swale
340	linear valley
341	pond, long and narrow
342	scarp, west-facing to 2 m
343	pond, continuous from south
344	pond; scarp, southwest-facing
345	swale
346	pond here to north; linear valley; swampy ground; east-facing scarp
347	swampy ground; scarp, northeast-facing; PH CP
348	pond, en echelon left-stepping
349	fault intersects road
350	pomd; linear valley to southeast
351	broad linear valley into lake
352	scarp, west-facing, to 2m; in road
353	abandonned outlet channel from pond
354	linear valley, flat-bottomed to south, steeper, narrower to north
355	linear stream drains southern lake
356	bench
357	scarp, east-facing; dried pond
358	bench, lower than bench to west
359	bench; traces east of pond fresher than traces here; western trace along pond, scalloped
360	bench
361	fault location uncertain; suspect along linear western edge of lake
362	pond, small, dry; linear swale to southeast
363	west-facing scarp
364	possible bench; no distinct fault features
365	swampy ground
366	gentle swale, east of ridge along lake
367	pond, east of ridge along lake; linear valley to southeast
368	scarp, east-facing, 2-3 m; east of redwood, west of new Plantation house; goes to 0 m
369	no scarp through pasture
370	offset tree; fault in road?
371	linear valley; scarp, east-facing to 4 m
372	bench, here to southeast
373	swampy ground; east-facing scarp to 5m
374	offset stream, ~10m; bench to south

Site	Feature Description
375	pond; scarp, east-facing, 8 m here, decreasing to southeast; linear valley
376	bench
377	scarp, east-facing to 1 m; abandonned channel west of fault
378	road crosses fault
379	bench; swampy ground
380	no clear fault features from south end of pond to canyon to south
381	bench; swampy ground
382	bench; linear valley with stream to south
383	linear valley
384	road
385	knickpoint; bench to north 100 m
386	bench, broad; trace unclear; knick point
387	scarp, northeast-facing; depression
388	scarp, southeast-facing; linear valley
389	scarp, southeast-facing; stream depositing across scarp
390	linear valley; depression; east-facing scarp
391	broad bench; scarp (1 m) buried by alluvium
392	fan from canyon behind east-facing scarp; broad bench to north (to CP 13-22)
393	bench below rd; W trace of 3 traces; middle trace along rd; eastern trace in linear valley
394	middle trace from N dies or merges w/ west trace
395	bench
396	pond; east-facing scarp on eastern trace
397	pond; swale; linear stream
398	bench from here NW
399	swale
400	swale on eastern trace; linear stream; stream deflection
401	pond; shallow swale to bench
402	pond
403	swale between E and W traces
404	narrow pond; swale
405	pond
406	pond; linear valley to SE; west-facing scarp to 3m
407	small pond with logs; swale between 12b-1 and 12b-2
408	bench
409	scarp to 4 m
410	pond along eastern trace
411	swale; east-facing scarp 1-2 m; pond 20 to south
412	south end of pond; 3 traces meet in pond; linear valley to south; east-facing scarp 2-3 m
413	pond
414	bench, possible trace in drainage; road
415	linear valley
416	wide (30 m) bench; scarp on west side

Site	Feature Description
417	linear valley draining southeast; east-facing scarp; N35W
418	pond; swampy ground
419	swale
420	broad bench, trace?
421	linear valley with steam and ponding
422	narrow swale to bench
423	linear stream
424	broad swale, possible trace
425	linear valley with stream; fault in stream
426	offset channel, modified by road; abandonned channel
427	linear trough; east-facing scarp
428	pond
429	pond
430	pond; broad linear valley
431	swale; broad scarp 2-3 m; dry pond to north
432	linear valley with intermittent ponding
433	linear valley
434	small pond (10 x1 m); more small ponds to south
435	southest end of long pond; linear stream to southeast
436	swampy ground in linear stream; pond to southeast
437	pond; linear stream and ponds to northwest
438	pond continues from point to NW
439	pond continues from point to NW and SE
440	S end of pond; linear valley to south with N-flowing stream; east-facing scarp 2-3 m
441	linear valley with intermittent ponds; east-facing scarp to 6 m
442	pond; east-facing scarp 2-3 m on W edge
443	broad bench, trace?
444	pond; swampy ground; swale; ponded alluvium buries scarp; trench site?
445	large pond, 10 m wide
446	broad swale; east-facing scarp, 8+ m, low and degraded to S; high sedimentation from drainage to E
447	broad swale with stream; trends into steep canyon
448	broad grassy flat bench, swampy ground, no clear fault trace; good trench site?
449	swampy ground
450	pond, developing from swampy ground to NW
451	headward erosion
452	swampy ground
453	bench, swampy ground; possible trace in canyon to W
454	broad linear valley with stream, steep eastern edge to bench to NW
455	swampy ground
456	broad bench
457	fault right step?

Site	Feature Description
458	gouge; erosion
459	fault poorly defined; bench and break in slope
460	low east-facing scarp 1-2 m; blocks drainage; small fan at foot of scarp not offset
461	broad subdued linear swale, flattens northward; possible trace
462	offset stream, west flowing diverted to N85W, east-facing scarp to 4m; road along fault
463	east-facing scarp to 3 m; road along fault
464	swale
465	east-facing scarp; fault in road
466	linear valley w/ stream - trace?; stream flow surfaces; east-facing scarp
467	east-facing scarp; ponded alluvium against scarp
468	deep gully, headward erosion along east-facing scarp; sub-fan flow; trench site
469	ponded alluvium
470	swale; fault diverges from gully
471	head of linear stream
472	linear valley; east-facing scarp to 6 m
473	broad bench; to east is steep slope; possible trace
474	bench
475	east-facing scarp to 8 m; pond; linear valley or swale
476	bench
477	bench
478	broad swale
479	linear valley with stream, 50 ft deep; drains pond; drains to NW
480	west-facing scarp?
481	road, with scarp?
482	large pond
483	pond with drowned trees
484	steep west-facing scarp
485	pond with cut stumps
486	south end of pond
487	steep east-facing scarp; linear valley
488	fault? along west edge of hump; swale on strike from this
489	linear valley to south
490	swale
491	steep east-facing scarp to 8m; linear valley/swale to N; pond to N; W edge of pond leaves flt
492	linear valley; dried pond
493	large pond
494	bend or step in fault; fault is east of here
495	pond N of rd intersection
496	west-facing scarp
497	pond; east-facing scarp to 4 m
498	bench
499	east-facing scarp to 3 m; dried pond; linear valley

Site	Feature Description
500	linear valley; east-facing scarp to 3 m
501	no fault features from here east to JZ 11-406
502	offset hill? steep west-facing scarp to south
503	no fault features
504	swale; linear gully to south
505	bench and road
506	swale in road, fault?
507	no fault features from here west to JZ 11-405
508	bench
509	bench w/ rd; spring; west-facing scarp
510	swale in road, fault?
511	bench
512	west-facing scarp modified by road; possibly connected to bench to NNW?
513	steep east-facing scarp; fault? or stream cut? swale to S; scarp diverges from stream
514	bench from here SE to spring; fault?
515	swale in road, fault?
516	anthrogogenic alteration has obscured any fault features
517	linear valley, east-facing scarp
518	linear valley, with stream, drains north
519	linear stream deflected; road
520	bench, modified by roads
521	spring; small pond; bench
522	linear valley; west-facing scarp; stream deflected north along W side of ridge to E
523	west-facing scarp to 5 m; modified
524	small east-facing scarp, NW strike turns to E-W
525	sw; 1906 trace?
526	west-facing scarp
527	shallow swale
528	swale
529	broad swale
530	swale, changing to flat at ridge top
531	small dry pond; swale
532	depression; west-facing scarp
533	swale, poorly defined to NW
534	east-facing scarp, degraded; break in slope
535	bench, west-facing scarp
536	broad swale with east-facing scarp to 6 m
537	bench, east-facing scarp, small depression
538	west-facing scarp
539	small dried pond
540	linear valley, possible trace, less active than trace to E?
541	swale
542	ponded alluvium, burying fence posts; fault maybe E of base of scarp; trench site?
543	ponded alluvium burying trees; small dry pond, trench site?

Site	Feature Description
544	swale, drains to W
545	small pond, active sedimentation
546	east facing scarp to broad swale west of stream
547	swale from here southeast, between CP 10a-6 and CP 10a-7
548	bench
549	bench
550	bench
551	pond, linear valley from here southeast 150 m
552	bench ends to SE; small west-facing scarp; poor expression
553	bench
554	bench, with parallel swale to west
555	deflected/offset drainage, 4 m; possible 1906
556	swale
557	linear valley, east-facing scarp to 3m
558	pond; to NW series of dry ponds in linear valley
559	stream deflection, 8 m; traces poorly defined across stream
560	linear trough, east-facing scarp
561	abandonned channel
562	linear valley; east-facing scarp subdued
563	swale
564	gouge exposed in stream cut; trough to E
565	drainage flows though here in narrow deep slot along fault
566	linear valley to canyon edge
567	linear valley, subdued trace, nothing clear between this point and traces to east
568	linear valley, swampy ground
569	linear valley, east-facing scarp to 4 m 40-50 m west of pond
570	east-facing scarp along road
571	W trace: broad bench, less defined to south; E trace in gully
572	pond, linear valley to south, steep east-facing scarp to 8 m; east trace dying to NW
573	east-facing scarp; linear valley; another trace to west
574	pond, swampy ground
575	swale to bench; scarp
576	bench, swampy ground
577	broad bench
578	broad bench
579	bench
580	bench, here NW to CP 10b-22
581	small pond
582	broad bench, swampy ground and grasses
583	west-facing scarp; bench below
584	dried pond; linear valley to NW
585	pond
586	west-facing scarp to 3 m

Site	Feature Description
587	low east-facing scarp
588	linear valley, east-facing scarp to 5 m; on scarp, 2 stumps (orig 1?); offset 2.7-3.1 m
589	east-facing scarp
590	linear valley
591	broad bench
592	bench
593	bench
594	swale; small left step; drainages sub-parallel to trace
595	east-facing scarp to SE; swampy ground to NW; bench
596	bench
597	linear valley w/ pond; east-facing scarp to 2 m
598	bench
599	pond on eastern trace; bench to swale; swampy ground
600	bench with log landing
601	offset stream, two traces
602	bench
603	large pond, two traces strike into edges of pond
604	pond in linear valley
605	bench; no clear fault features
606	linear valley; small pond to NW
607	swampy ground with road
608	splay, N20W strike, east-facing, 1-2 m
609	linear valley
610	linear valley, w/ east-facing scarp
611	broad bench, trace subtle
612	bench becoming swale, diverges from stream
613	swampy ground, west-facing scarp to 10 m; site of triangular array
614	west-facing scarp; swampy ground ot west; N35W
615	Buttermore Ranch
616	bench
617	scarp, west facing
618	scarp, west facing, welldefined, to 3 m
619	broad bench; fault in deep gully to west?
620	bench, meets gully to south
621	no clear fault features; fault in drainage?
622	no clear fault features; fault in drainage?; huge boulders in confluence
623	slump edge; fault in gully to west?
624	landslides ubiquitous; fault features obscured
625	broad bench, fault-related?
626	bench, poorly developed
627	broad bench
628	no clear fault-related features
629	scarp, east facing, to 10 m

Site	Feature Description
630	broad swale, flattening to south
631	swale
632	broad bench, > 50 m wide
633	bench and swale, less well-defined than next bench east; possible fault
634	bench
635	pond, linear valley
636	linear valley
637	no fault features evident
638	road and bench; possible trace in road to SE?
639	linear valley, southern end; bench to S
640	bench and road
641	broad bench with road; trace?
642	RL jog in stream; fault gouge exposure
643	spring
644	bench (and road); spring
645	swale, broad
646	pond; linear valley; scarp, west facing
647	pond; scarp, east facing
648	gouge?
649	scarp, east facing to 4 m; pond, ephemeral; swale
650	swale
651	pond, ephemeral; swales and ponds here to CP 9-26; topped trees to W
652	pond; ponded alluvium; ponded darinage
653	swale
654	gentle swale
655	swale, very subtle
656	swale continues
657	linear valley; scarp, east facing to 3 m; distorted trees
658	scarp, east facing, modified by road
659	scarp, east facing; swale
660	steep scarp, east facing; pond
661	swale
662	scarp changes to west-facing to S; head of gully
663	pond, modified; east-facing scarp; 1906 Lawson - offset wagon rd
664	offset stream channel; scarp cut back, before stream incised?
665	scarp, east facing, ~150-200 m
666	scarp, steep, east facing, to 5m
667	broad bench; swale
668	swale to bench; west-facing scarp
669	bench
670	broad swale
671	bench; fault uncertain
672	bench

Figure 1. Map of northern California and Quaternary faults included in the U.S. Geological Survey Quaternary fault and fold database (USGS/CGS, 2006). Base image from Google Earth.

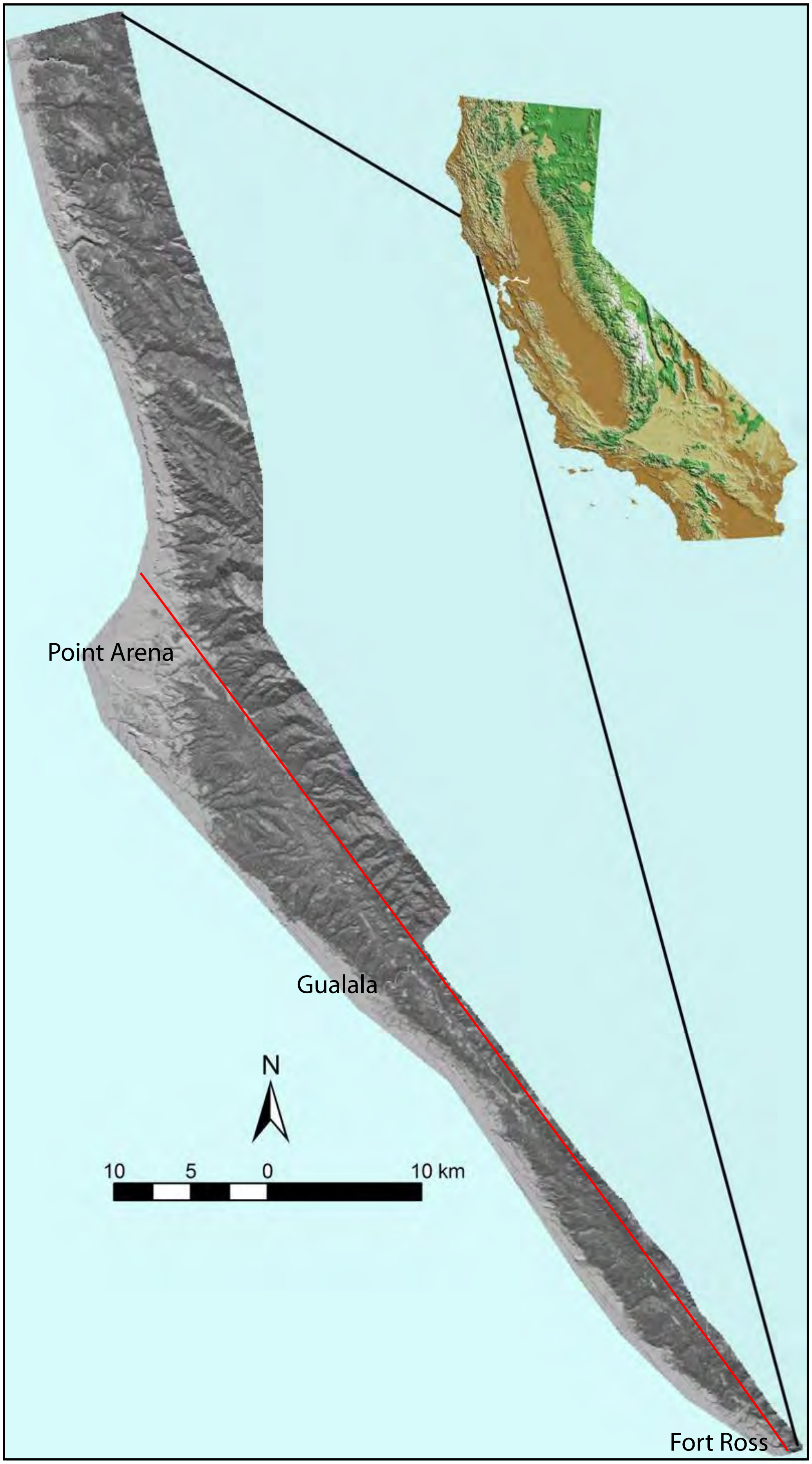

Figure 2. Extent of 2003 Lidar survey. Red line marks approximate location of the San Andreas fault.

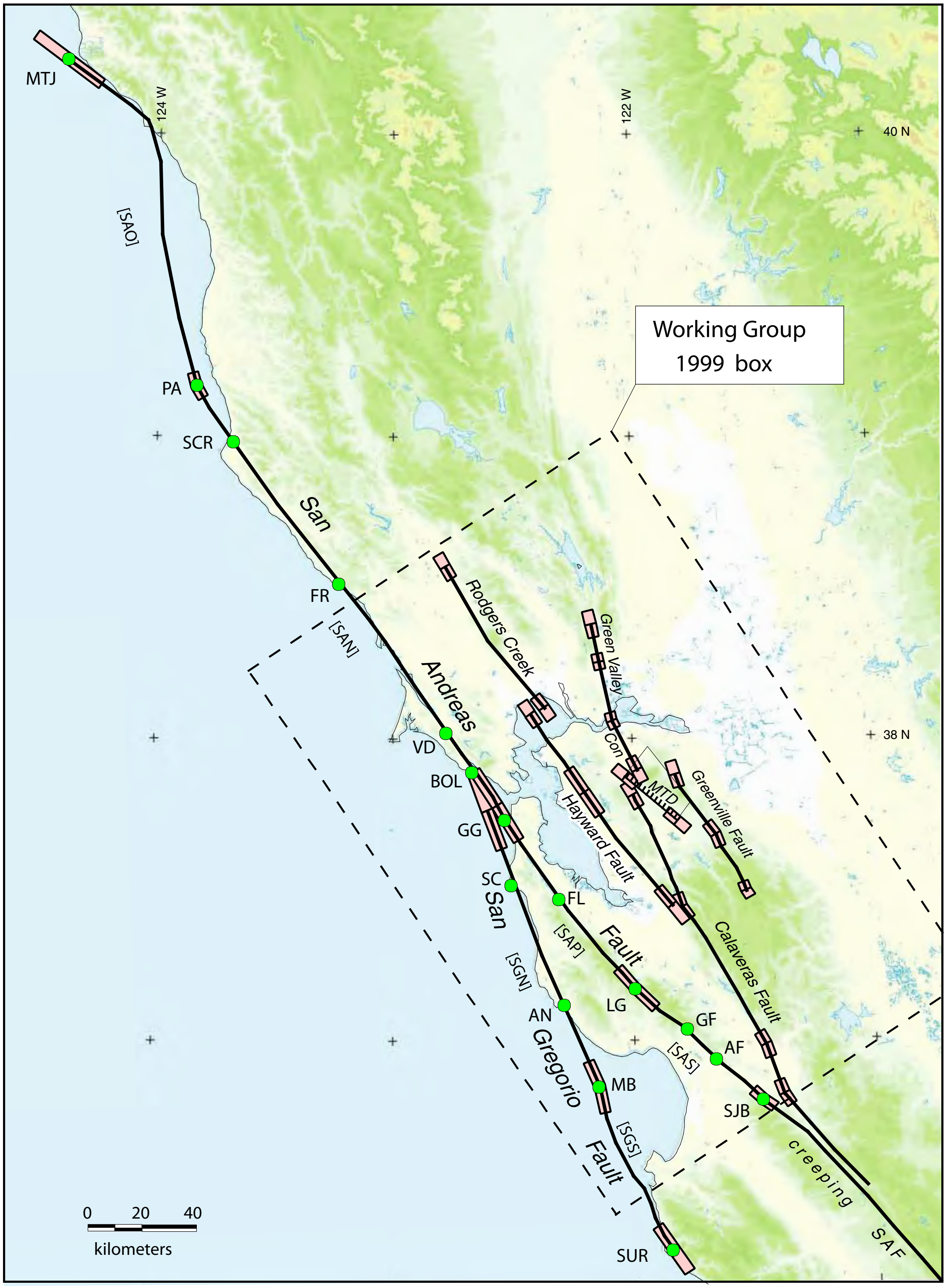

Figure 3. Map of fault segments defined by the WGCEP (2003). The San Andreas fault include four segments from north to south: Offshore (SAO), North Coast (SAN), Peninsula (SAP), and Santa Cruz Mountains (SAS). Other features discussed in the text include: PA (Point Arena), FR (Fort Ross), VD (Vedanta), SJB (San Juan Bautista). Figure from WGCEP (2003).

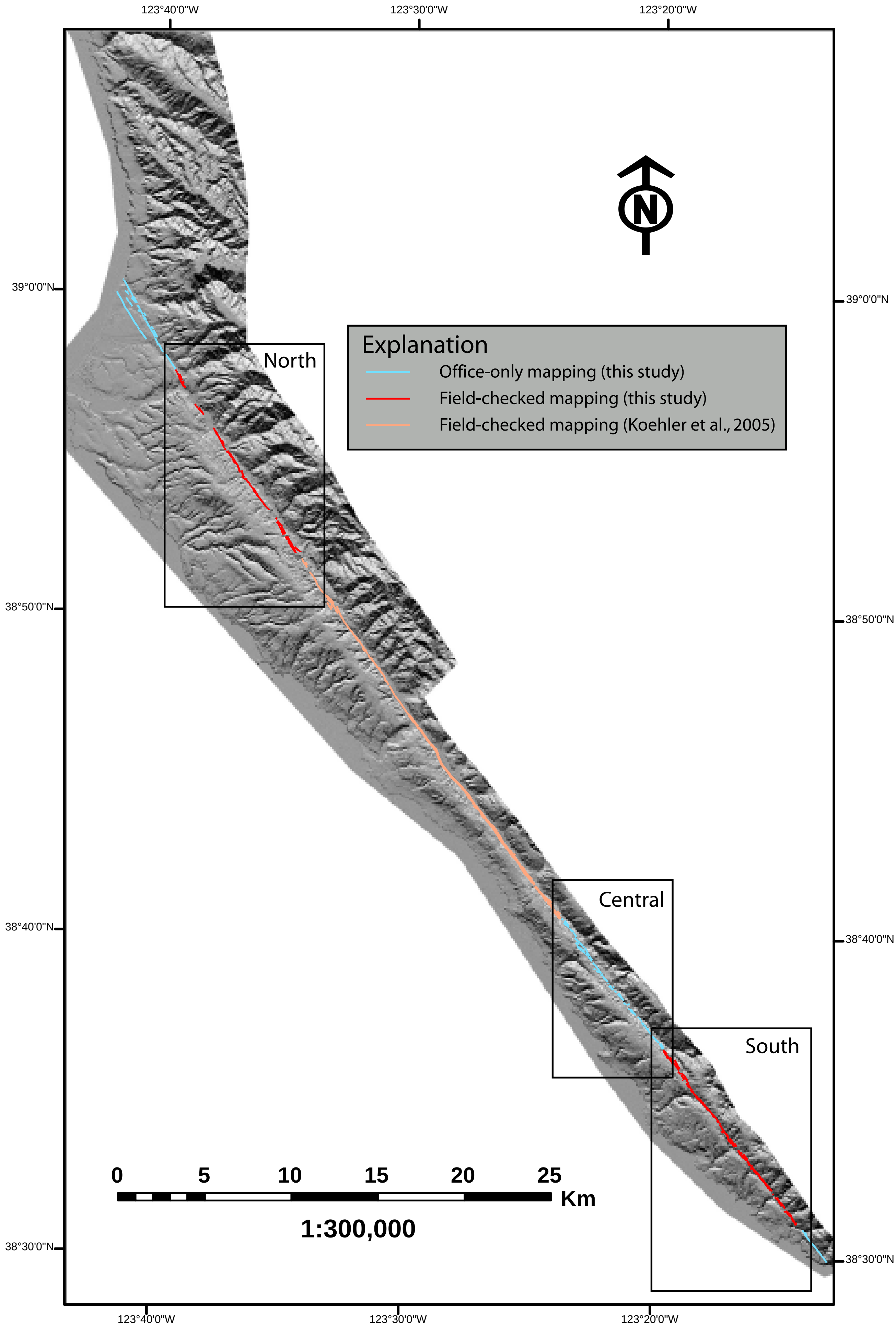

Figure 4. Study area, with sections discussed in text, shown on LiDAR DEM. North and South sections shown in Figures 5 and 6; Central section shown in Figure 15.

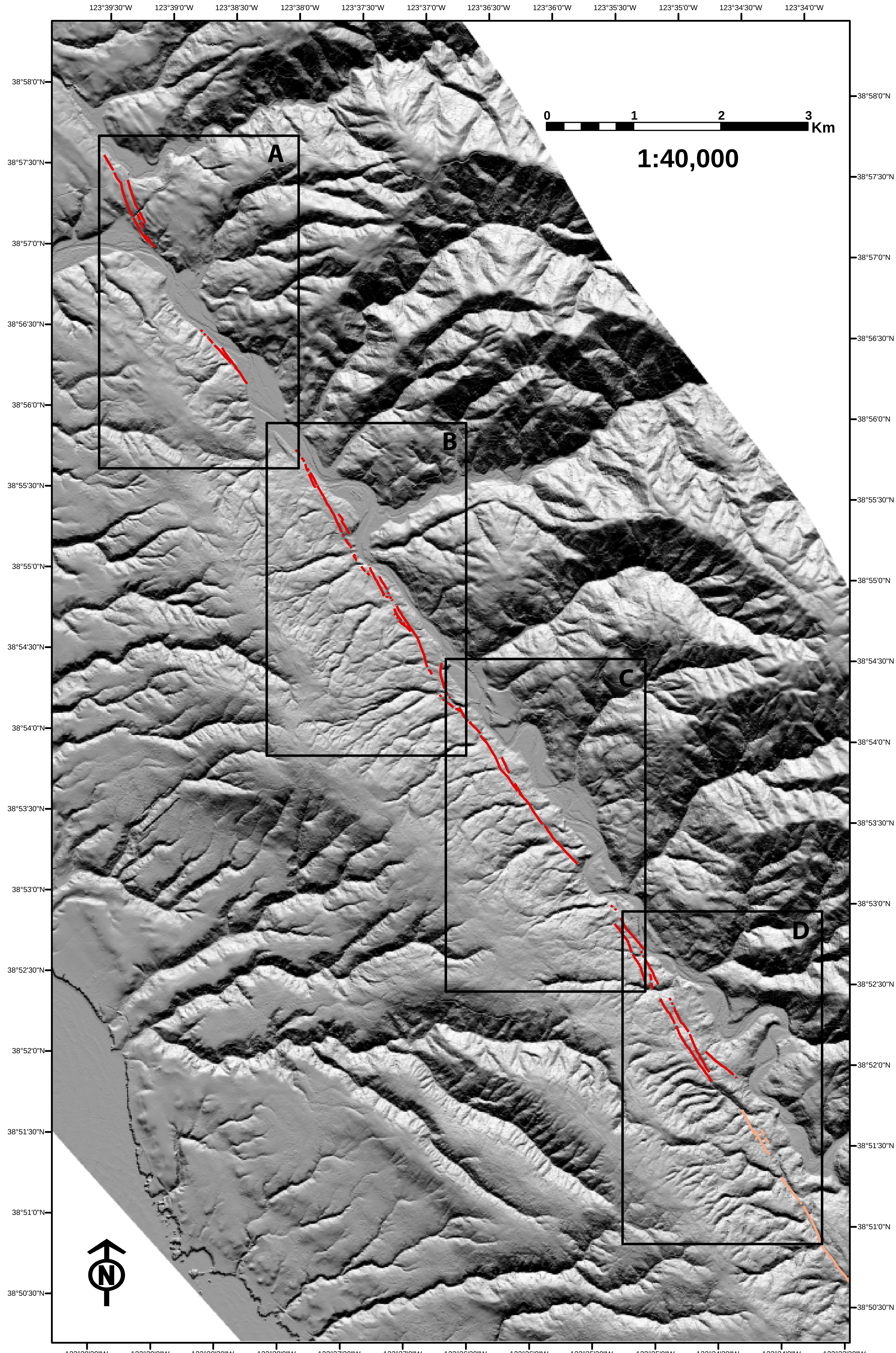

Figure 5a. Mapping in the northern section. Boxes outline detailed 1:10,000-scale mapping shown in Figures 6a-d.

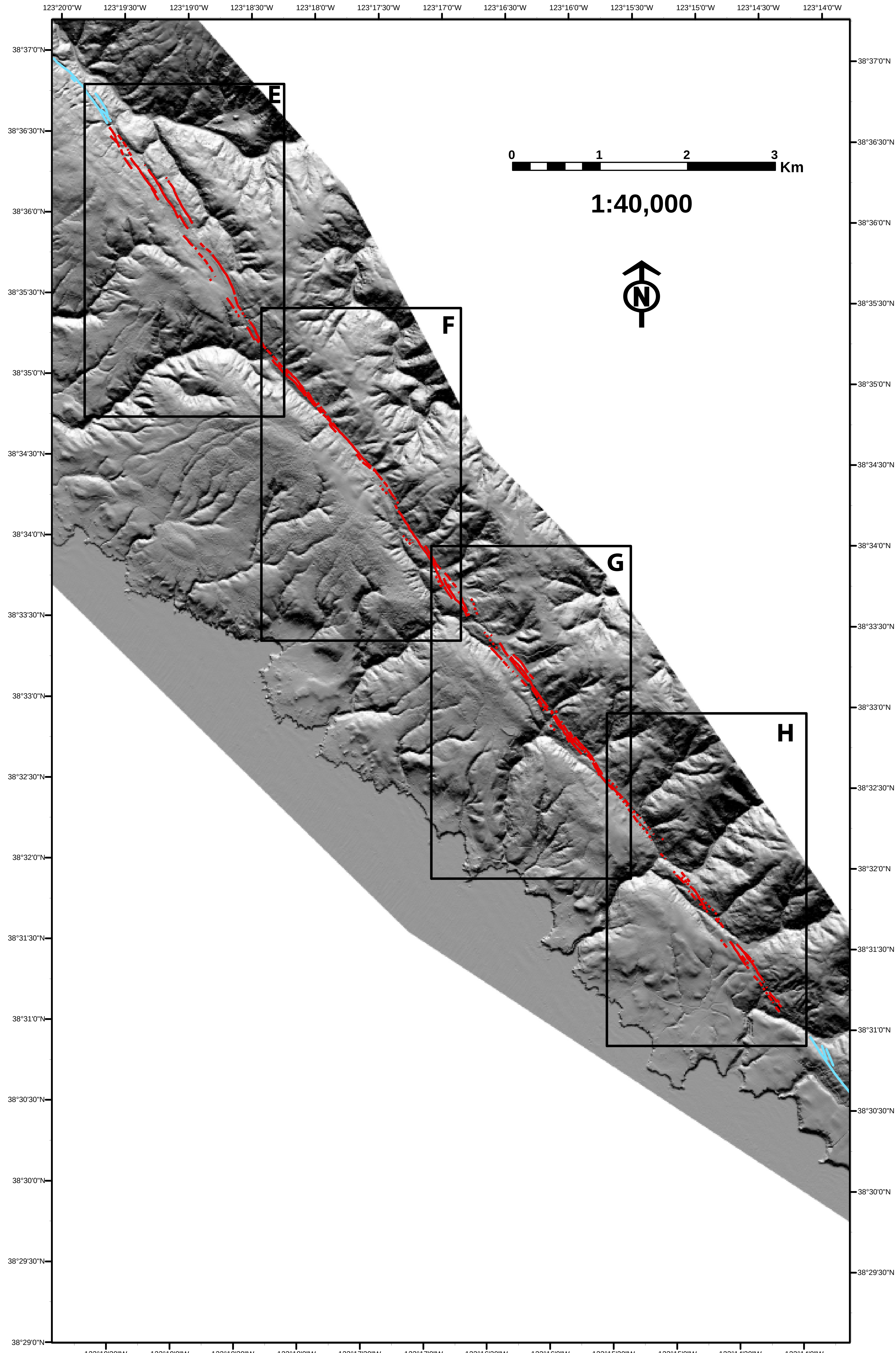

Figure 5b. Mapping in the southern section. Boxes outline detailed 1:10,000-scale mapping shown in Figures 6e-h.

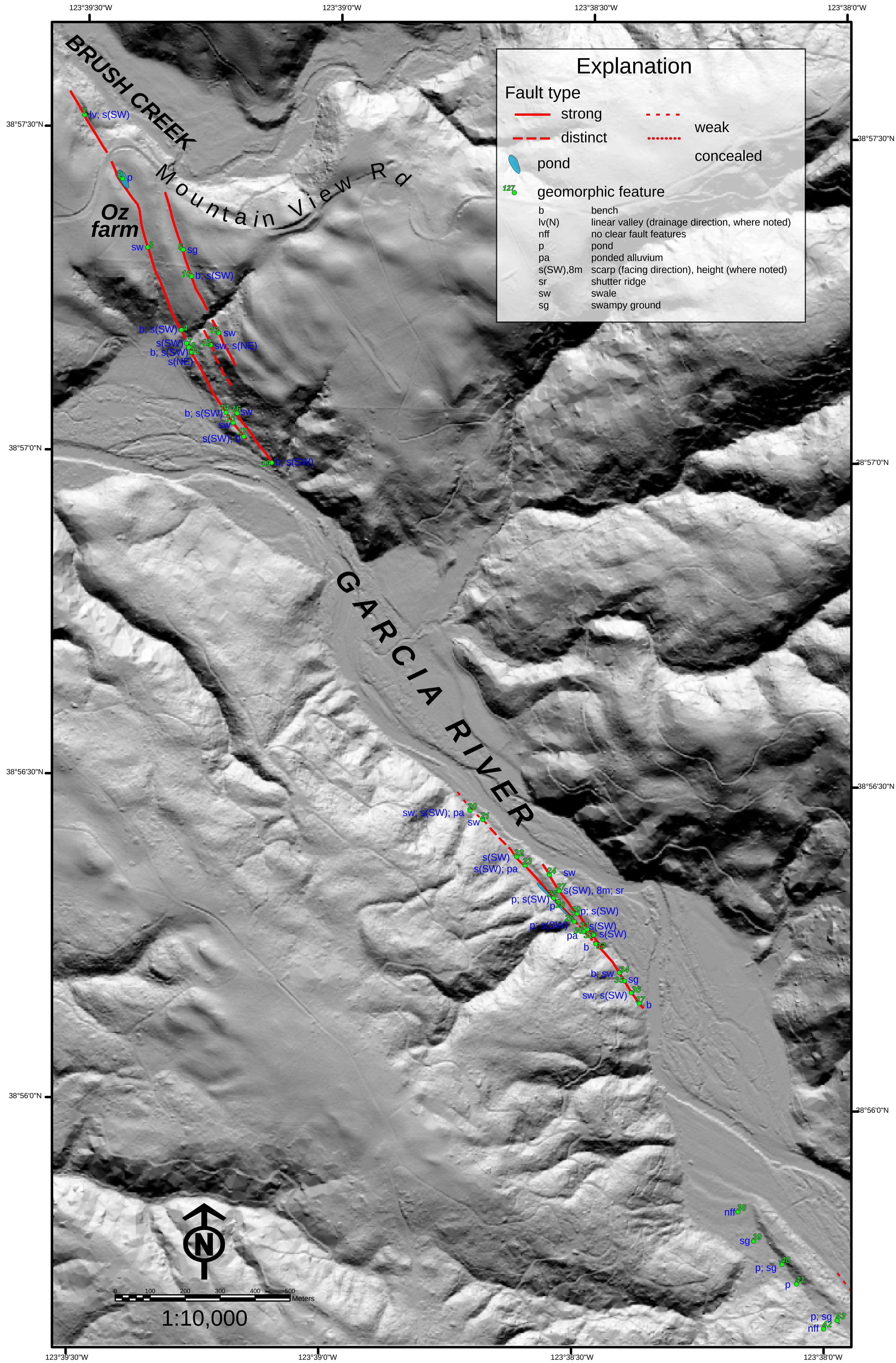

Figure 6a. Mapping in Oz Farm section.

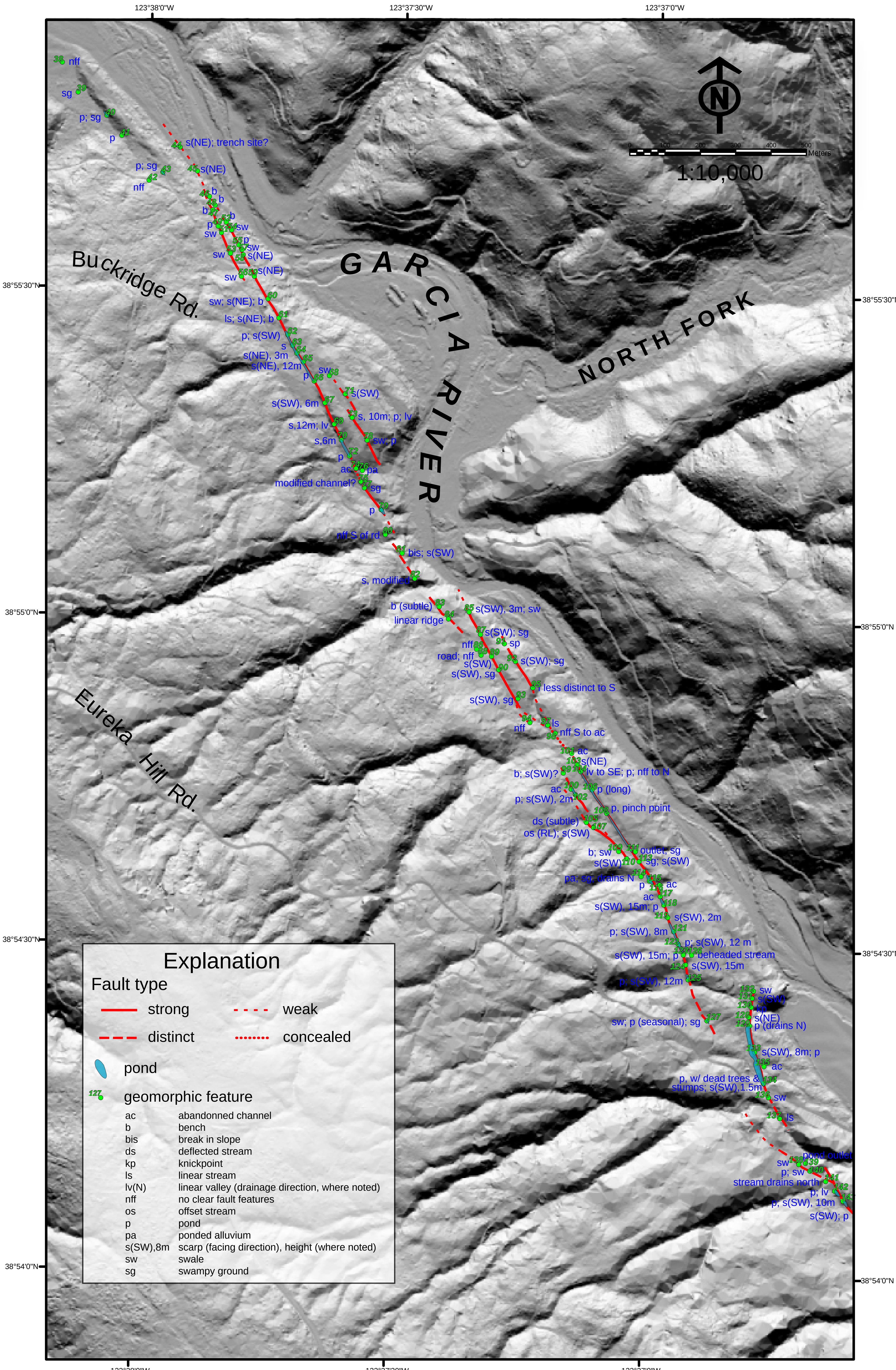

Figure 6b. Mapping in Eureka Hill Road section.

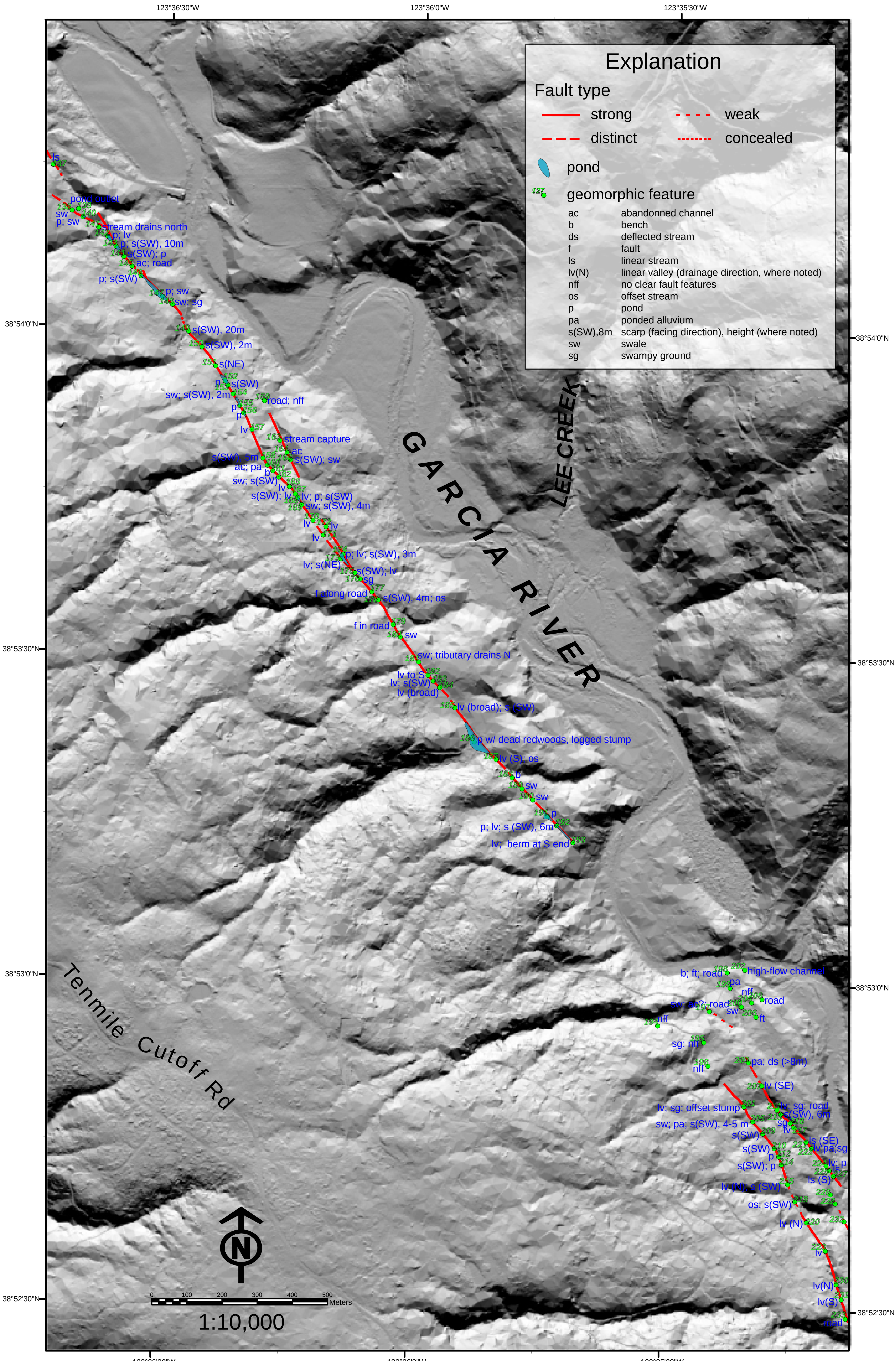

Figure 6c. Mapping in Lee Creek section.

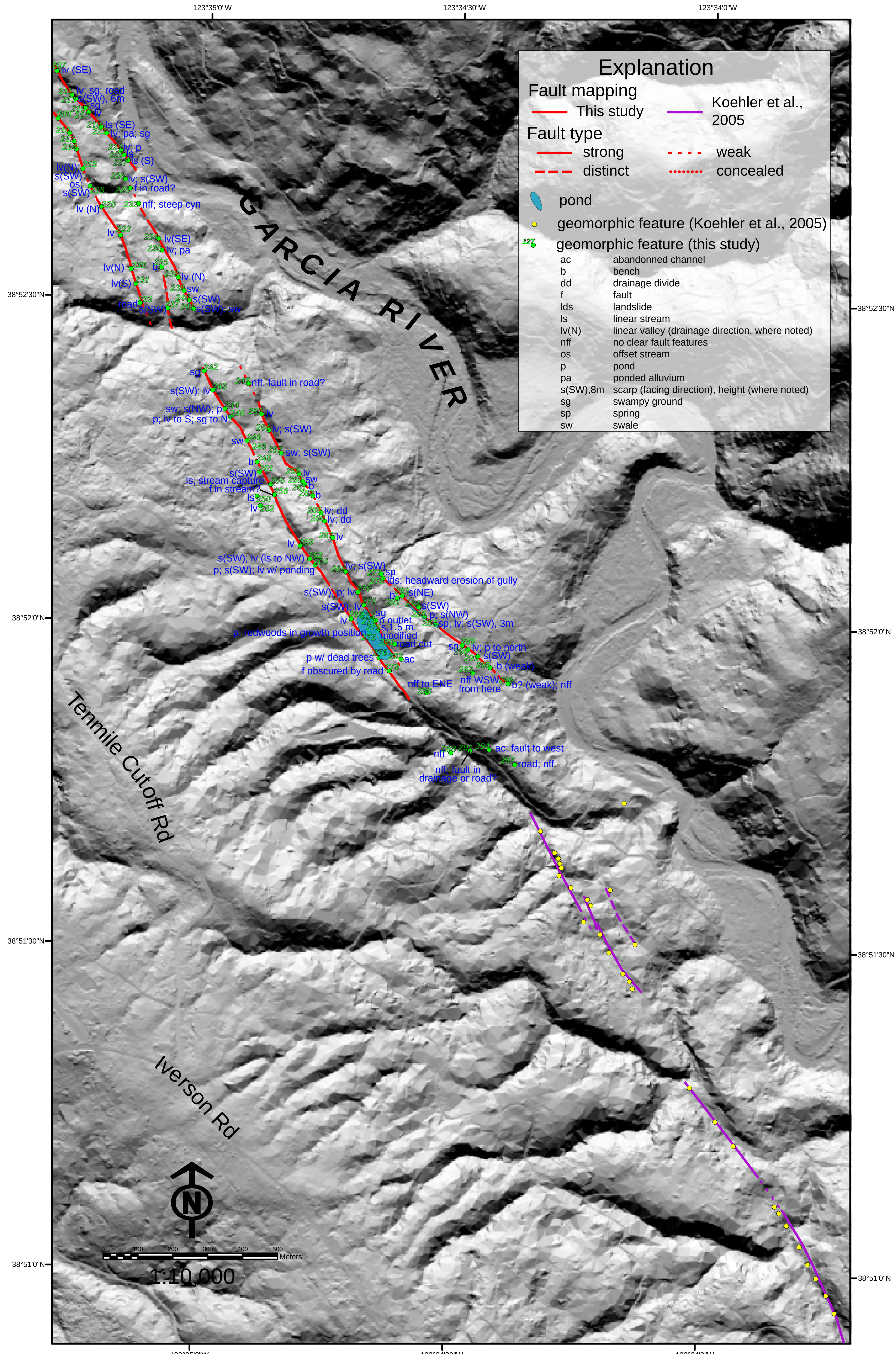

Figure 6d. Mapping in Iverson Road section.

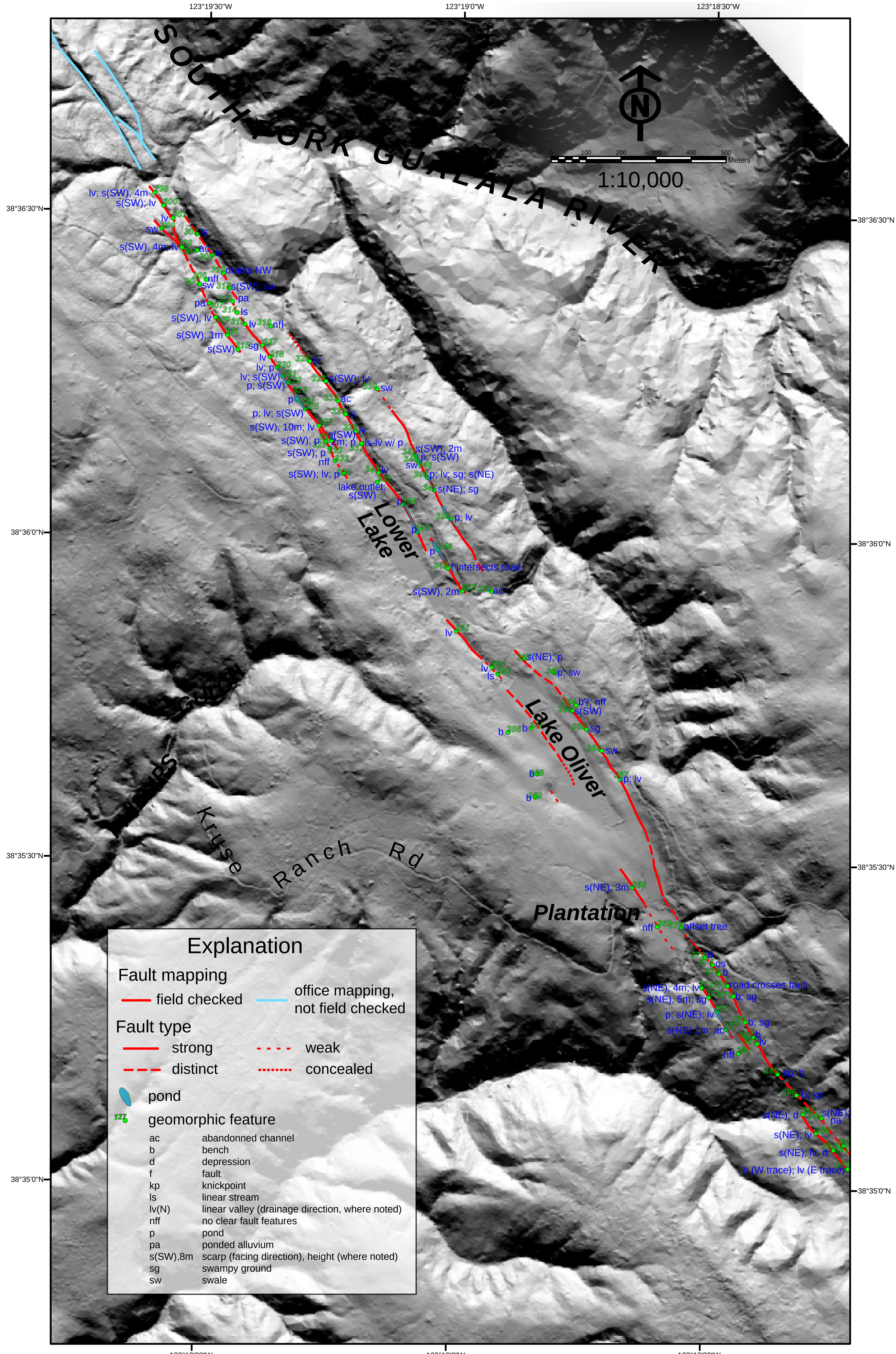

Figure 6e. Mapping in Plantation section.

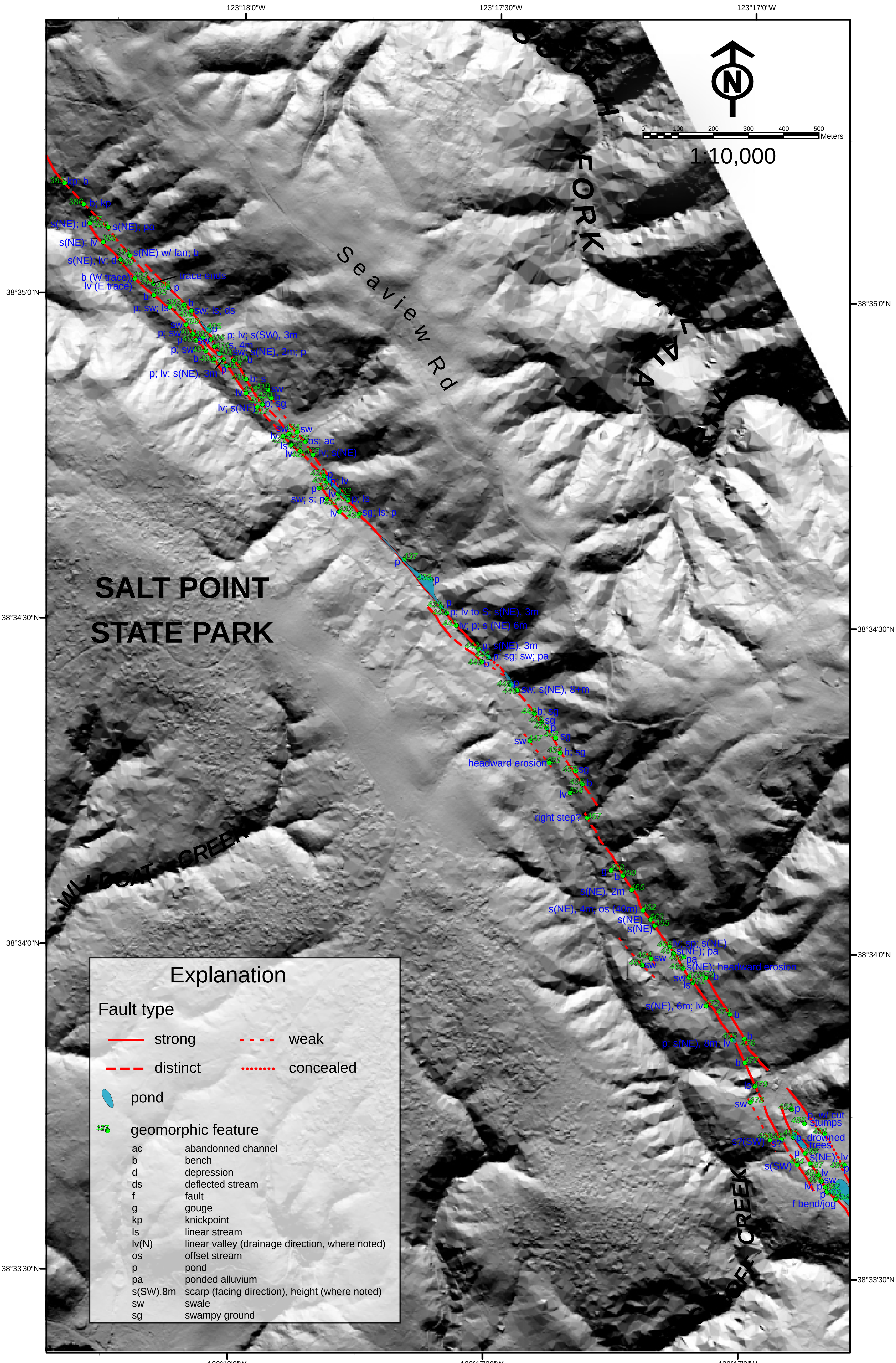

Figure 6f. Mapping in Salt Point State Park section.

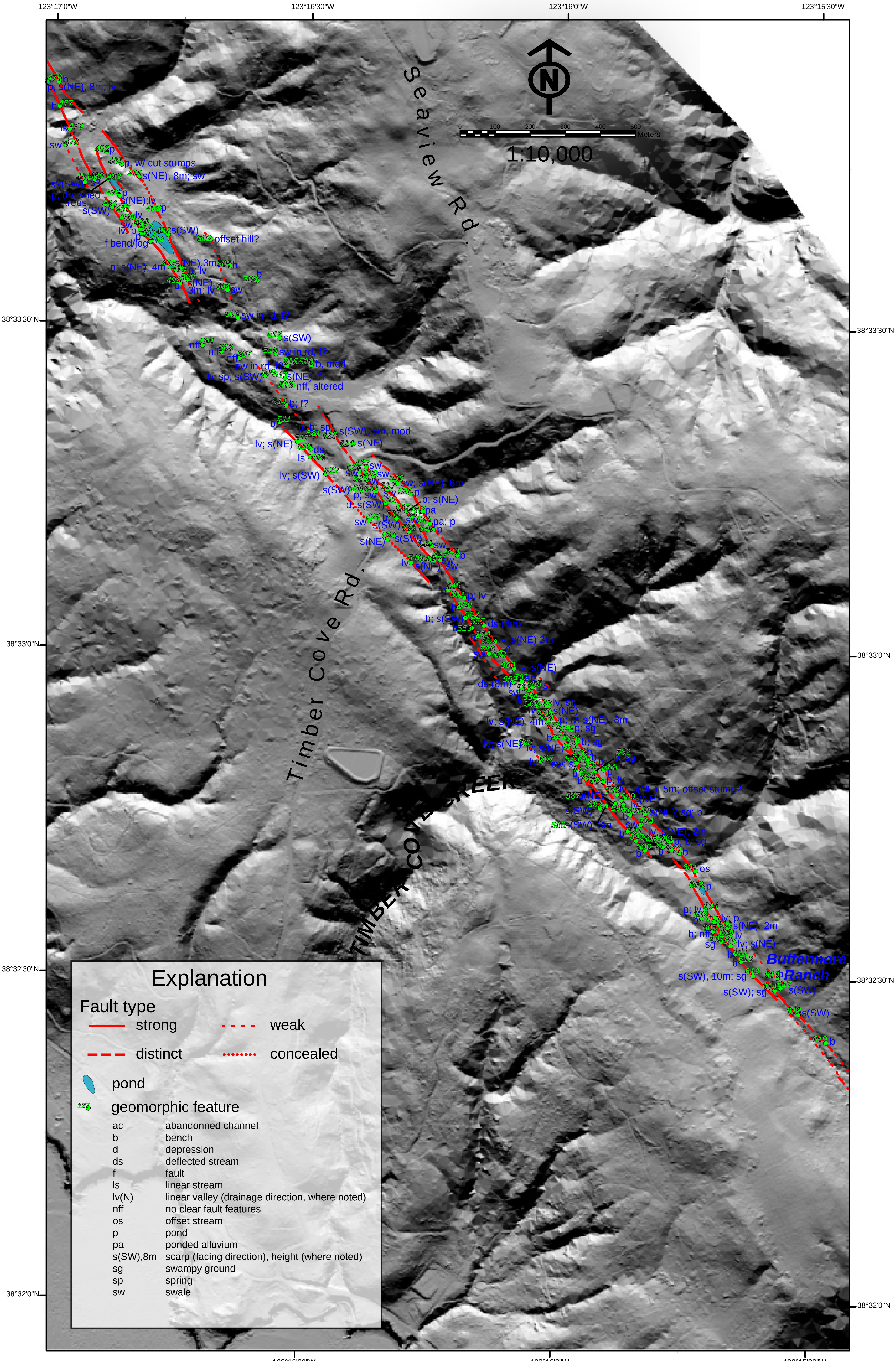

Figure 6g. Mapping in Timber Cover Road section.

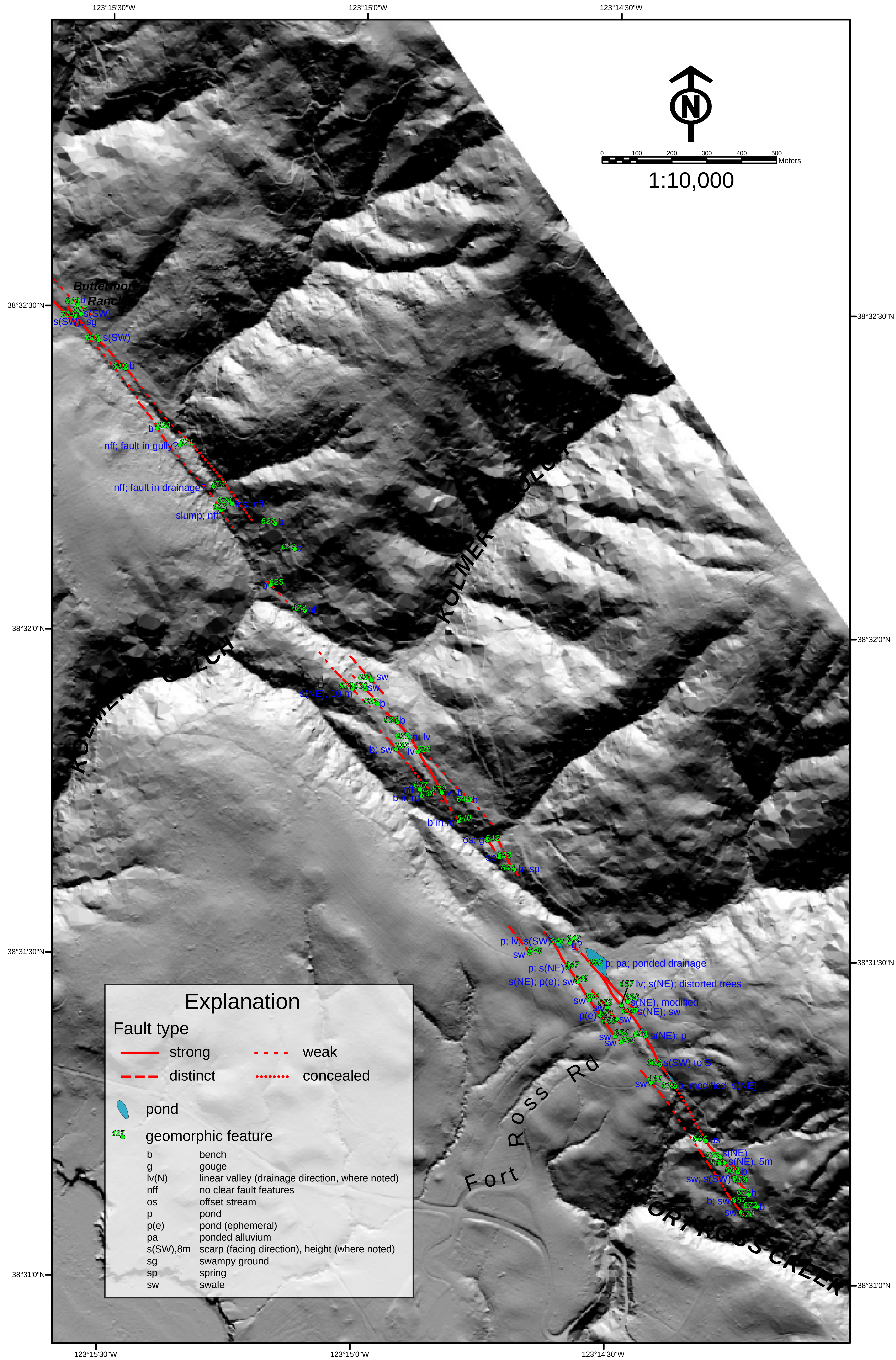

Figure 6h. Mapping in Fort Ross section.

Figure 7. Photograph of pond along fault with drowned trees. Site 134, Figure 6b. View to the northwest.

Figure 8. Linear valley along fault. Site 182, Figure 6c. View to the southeast.

Figure 9a. Burned and twice-offset logged redwood stump. Red arrows marked logged top surface of stump and illustrate vertical separation of two sides. View to south.

Figure 9b. Split cavity in offset stump, with view to the northwest. Red arrows mark vertically separated tops of logged stump; red box marks location of detailed view in Figure 9c.

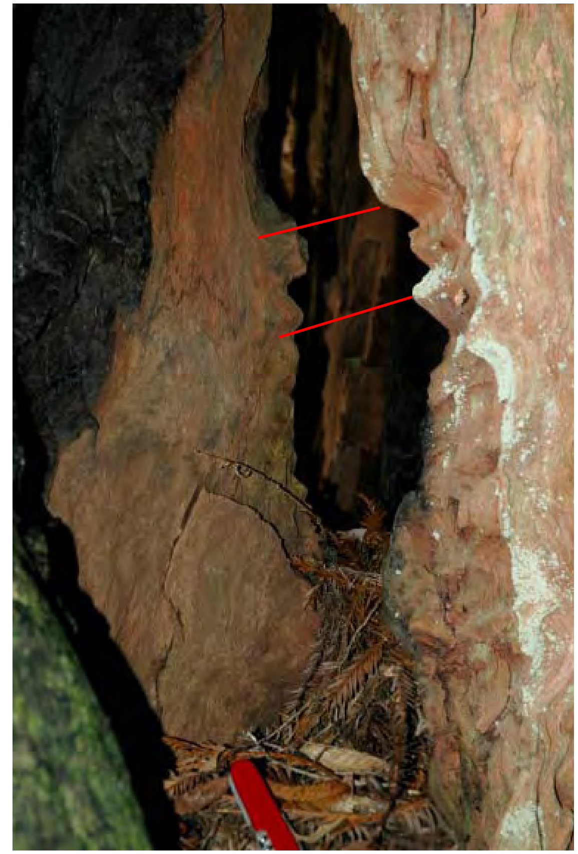

9c. Close-up of interior of split in offset stump. Offset "puzzle pieces" match precisely and indicate nearly horizontal displacement, smaller than total stump displacement.


Figure 10. Linear valley with small pond. Site 259, Figire 6d. View to the northwest


Figure 11. Linear valley with west-facing scarp that reaches 10 m in height. Site 327, Figure 6e. View to the northwest.

Figure 12. Tree on road at Plantation farm offset in 1906 earthquake. Site 370, Figure 6e. View to the south.

Figure 13. West-facing scarp at Buttermore Ranch. Site 614, Figure 6g. View to the southeast.

Figure 14. Trees damaged in 1906 earthquake. Near Fort Ross Road. Site 653, Figure 6h. View to the southwest.

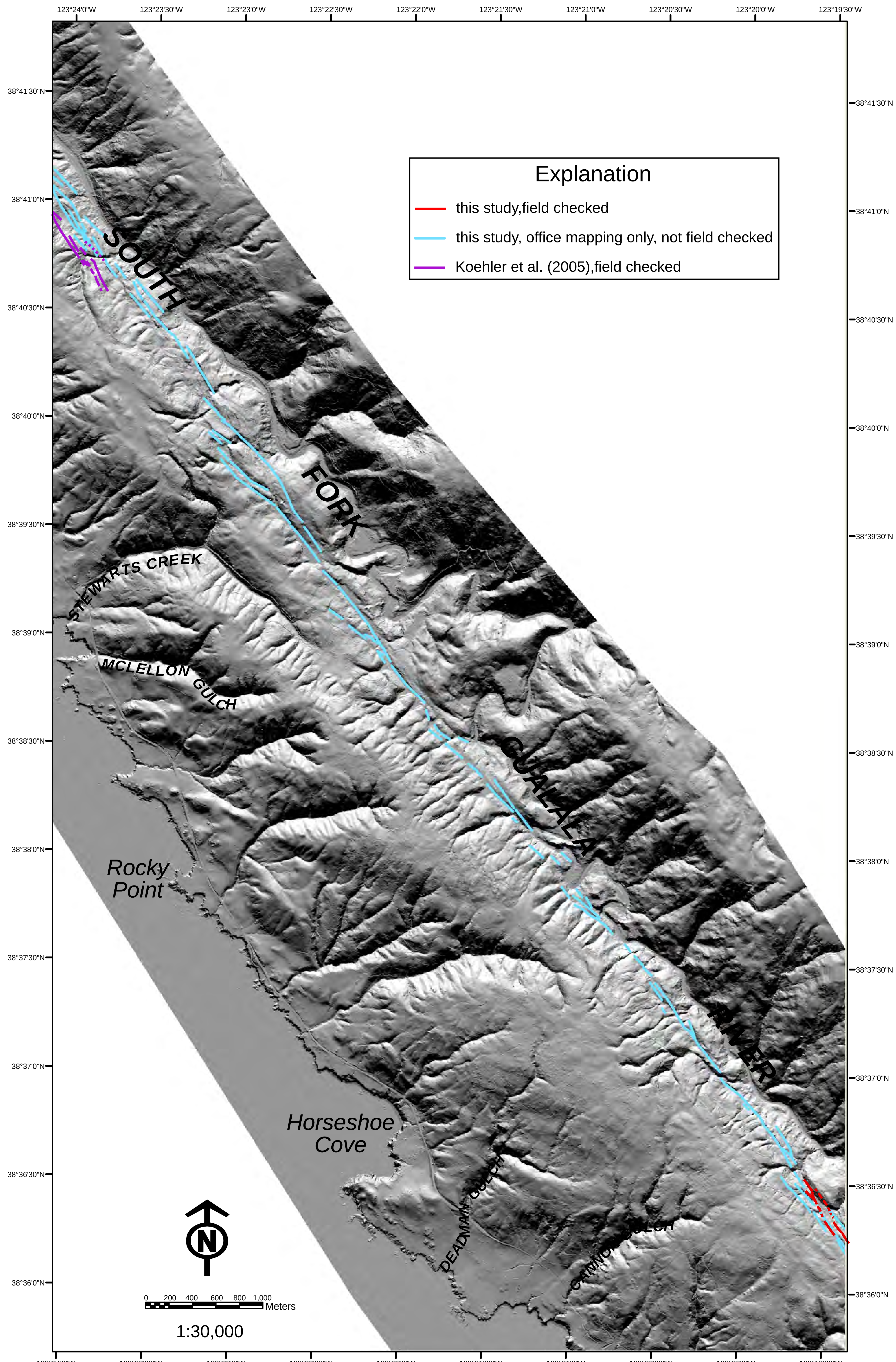

Figure 15. Mapping in the central section with no field checking.

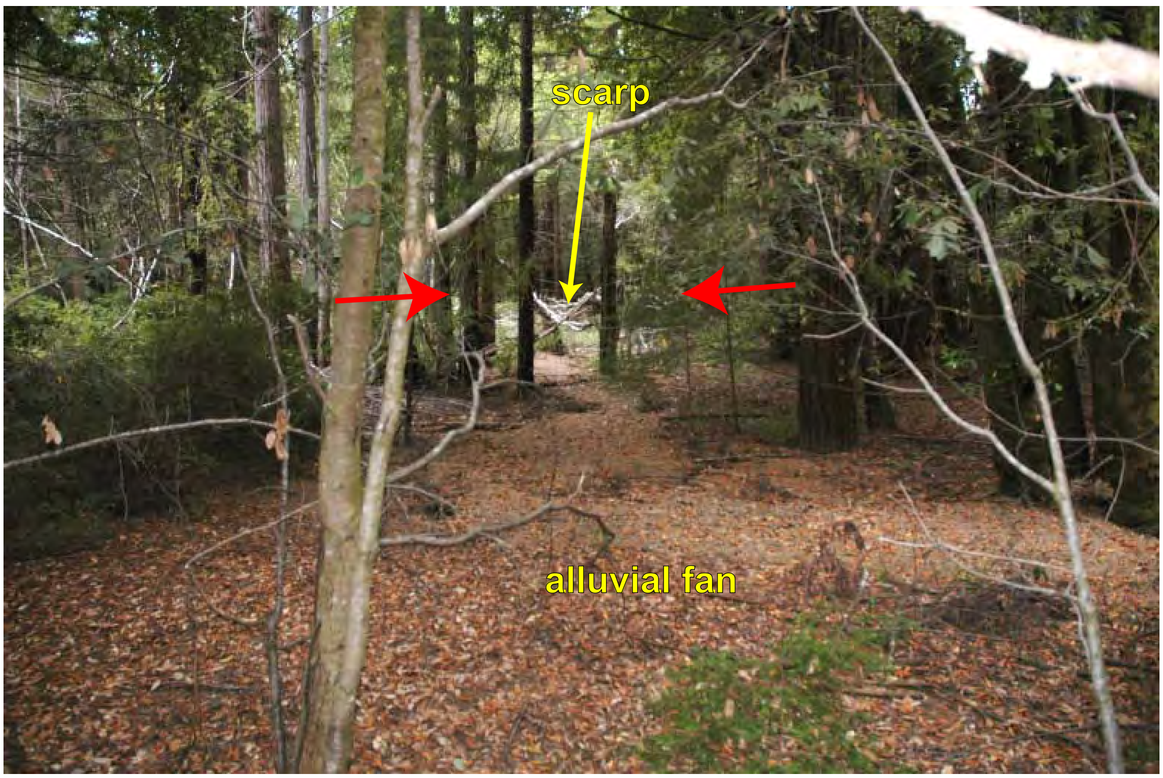

Figure 16. Possible trench site where Holocene alluvial fan material is deposited against a east-facing fault scarp in Salt Point State Park. Site 467, Figure 6f. View to the west. Red arrows mark the fault; fellow arrow points to the buried scarp.